University of South Carolina

Scholar Commons

Spring 2020

Investigating the Effects of Aggregate Size and Reinforcement on ASR Cracking in Concrete Structures Studied with Different Evaluation Methods

David Joseph Bianco

Investigating the Effects of Aggregate Size and Reinforcement on ASR Cracking in
Concrete Structures Studied with Different Evaluation Methods

By

David Joseph Bianco

Bachelor of Science
University of South Carolina, 2018

_____

Submitted in Partial Fulfillment of the Requirements

For the Degree of Master of Science in

Civil Engineering

College of Engineering and Computing

2020

Accepted by:

Paul Ziehl, Director of Thesis

Robert Mullen, Reader

Sarah Gassman, Reader

Cheryl L. Addy, Vice Provost and Dean of the Graduate School

www.manaraa.com

DEDICATION

I dedicate this thesis to my family. Mom, Dad, and Jenna, thank you so much for your everlasting support in everything that I do. You are the reason I am the man I am today, and the reason I can achieve anything I put my mind to. I want to specifically thank my mother for doing anything necessary to allow me to reach my goals and being the best mother I could have ever asked for. Dad, thank you for being my role model. You are the most hard-working, genuine, brilliant man that I have ever met, and you have provided me with endless support throughout my entire life. Words cannot describe how much I love and appreciate you guys, so thank you.

ACKNOWLEDGEMENTS

I would like to acknowledge my research colleagues I had the chance to work with and learn from during my time in graduate school and this includes: Rafal Anay, Robert Moore, Vafa Soltangharaei, Li Ai, Brenna Feirer, and Mahmoud Bahyat.

I'd like to thank all my friends that I have made at USC because I would not be who I am without them. Also, I would like to acknowledge the incredibly university that has allowed me the opportunities to grow as a student, man, and engineer.

I would also like to thank all of my undergraduate professors for providing me the body of knowledge that I have used to develop into the engineer I want to be, and this includes: Dr. Juan Caicedo, Dr. Fabio Matta, Dr. Michael Meadows (DOP), Dr. Robert Mullen, and Dr. Charles Pierce.

Lastly, I would like to put forth a sincere gratitude towards Dr. Ziehl. Thank you for allowing me the opportunity to work on a multitude of projects and diversify my experience in the realm of structural engineering. I would not have the opportunities I have today without you.

ABSTRACT

The objective of this thesis is to investigate different (non-destructive) evaluation methods to assess the effects of reactive aggregate size and reinforcement on ASR affected concrete. It has been shown in previous literature that reactive coarse aggregates lead to more expansion as opposed to reactive fine aggregates. However, there is a lack in the literature exhibiting this relationship using different evaluation methods, such as acoustic emission (AE) and ultrasonic pulse velocity (UPV). Also, the literature does not emphasize the role this relationship plays when the concrete is imposed with stress boundary conditions. Non-destructive test methods, including acoustic emission, are becoming a more widely used method of testing concrete, so this thesis will investigate how these non-destructive evaluation methods reflect early ASR damage in concrete; the methods will also help to further understand the roles aggregate size and reinforcement play in ASR infected concrete's degradation process.

The tests elaborated on in this thesis were completed over two and a half years. Each test has one confined, one unconfined, and one control specimen. The confined specimen is fitted with steel reinforcement. The coarse reactive coarse aggregate concrete was initially tested to understand the affect boundary conditions have on the ASR reaction. The results of this thesis show that the unconfined reactive fine specimen experienced isotropic expansion. In addition, the effect of reinforcement is more pronounced in the reactive coarse aggregate specimens than in the reactive fine specimens. When evaluating the non-destructive test methods in terms of contrasting damage between the reactive and

control specimens, the evaluation methods are ranked as follows (largest difference to smallest difference): acoustic emission (cumulative signal strength), expansion measurements, visual crack measurements, followed by UPV.

The novelty of this thesis comes from the innovative method of evaluating the accuracy of different non-destructive test methods for ASR affected concrete, as well as investigating the effects of reinforcement and different aggregate sizes on ASR affected concrete with the non-destructive (most notably acoustic emission) test methods.

TABLE OF CONTENTS

LIST OF TABLES

LIST OF FIGURES

xi

LIST OF ABBREVIATIONS

AASHTO .... American Association of State Highway and Transportation Officials

AE .... Acoustic Emission

ASR .... Alkali-Silica Reaction

ASTM .... American Society for Testing and Materials

FFT .... Fast Fourier Transform

FHWA .... Federal Highway Administration

ITZ .... Interfacial Transition Zone

RCAC .... Reactive Coarse Aggregate Concrete

RFAC .... Reactive Fine Aggregate Concrete

UPV .... Ultrasonic Pulse Velocity

CHAPTER 1

Abstract and General Introduction

1.1: Layout of Thesis

This thesis is to be composed of five chapters. The first chapter is a general introduction to the topics that will be discussed throughout the paper. These topics include acoustic emission, concrete, the alkali-silica reaction, different non-destructive test methods, and an abstract for the thesis.

Chapter two consists of a literature review on research regarding the major aspects of this thesis, which also includes acoustic emission and ASR, mainly. This literature review also covers vocabulary related to AE that is used as well as many ASTM standards that are pertinent to ASR.

Chapter three presents the experiment and how it was set up. This includes the creation of the samples, the test setup, and the materials used to analyze the data.

Chapter four is the analysis portion of the thesis. This chapter presents the test setup, information on how the test was performed and executed, and the results. The chapter also provides a discussion as to why the analysis and data looks the way it does. The results in this chapter are to be submitted to a major conference to be published independently.

Chapter five is the conclusion to this thesis that will summarize all the chapters that came before it. Recommendations for future work are also present in this chapter.

1.2: General Introduction

Concrete is used in a variety of different structures including nuclear power plants, bridges, dams, and residential and commercial buildings. As a widely used building material it is susceptible to many different conditions as well including rain, snow, heat, humidity, and radiation. Concrete is made up of mainly 4 separate components, and with the variances in uses and the environments in which it is placed in there is a multitude of

www.manaraa.com

ways concrete can deteriorate or fail. These include corrosion of the steel reinforcement, freeze-thaw cycling, scaling, loading and cracking, sulfate attacks, salt crystallization, microbiological attacks, erosion, delamination, and the alkali-silica reaction. These degradation processes affect the sustainability, serviceability, and safety of the many types of structures built with concrete (Clifton 1991).

The alkali-silica reaction that occurs in concrete has been affecting concrete structures for nearly 8 decades. However, this problem has not typically been at the forefront of research until very recently. It became apparent at the Seabrook Nuclear Power Plant (NRC 2011) and academia has been researching why it is happening as well as ways to solve this problem. The degradation mechanism itself occurs at the chemical level during the creation of concrete but lasts and grows for the concrete's lifetime.

As this thesis is being written, the best way to avoid any problems relating to ASR is to utilize building materials that will not react. So, contractors and engineers should use aggregates that are less likely to have reactive silicas on their surface. However, this method is not as easy as it sounds. There are a few ASTM standards, including ASTM C1293 and ASTM C1260, that are widely used to screen aggregates for a potential ASR reaction. These methods are an improvement as compared to the previous ASTM C289 and ASTM 295 standards at detecting aggregates with a high reactivity, but many times they have still shown false positives and false negatives on aggregates that should be rejected or accepted, respectively. Although testing methods are improving with time, there is still no widely accepted way of defending new structures from a lifetime of degradation through the alkali-silica reaction.

The reaction itself occurs during the creation of concrete, and the gel that is formed continuously expands during the entire life of the structure. This expansion is what causes the concrete to crack and deteriorate. There are a few different ways to monitor the degradation and how impactful the ASR has been to certain structures. These methods include petrography, visual inspections, and coring. Visual inspections are clearly limited to just the surface of structures, while coring and petrography are destructive methods. Acoustic emission is a nondestructive testing mechanism that has been shown to monitor the degradation of ASR affected concrete (Jones 2013; Ziehl 2008). Long term monitoring of concrete can be done to understand how ASR is affected by different aggregate types, how different conditions affect ASR, and how reinforcement affects ASR affected concrete. The objective of this research is to understand, through the investigation of non-destructive methods, how concrete's aggregate size, and reinforcement design, affects the damage mechanisms of ASR.

CHAPTER 2

Literature Review

2.1: Alkali-Silica Reaction

Concrete, the world's most widely used building material, typically consists of four main constituents: coarse aggregates, fine aggregates, water, and cement. This study focuses on the reaction that occurs between the alkalis (mainly $NaOH$ and K_2O) found in the cement solutions and the silica (SiO_2) that is commonly found in aggregates. Water is the catalyst that excites the alkali-silica reaction to occur. Once the concrete's ingredients are combined and water is added, the alkali compounds in the cement split into hydroxyl ions (OH^-) (Lokajíček et al. 2017). These hydroxides then break the silica bond that is in the concrete and a gel like substance begins to form around the aggregates and on a microscopic scale. The reaction happens over time and effects are not always observed immediately. The gel is hydroscopic, so it will continue to expand over time in the presence of moisture or high relative humidity and temperature. The expansion of this gel around the aggregates is what leads to the microcracks, macrocracks, and visual deterioration common with ASR. See **Figure 2.1** for an example of the phenomenon known as map cracking, which is a type of visual deterioration seen in ASR affected concrete. There is

Figure 2.1: *ASR affected dam in Norway (Thomas 2013)*

currently no way to stop the reaction, but once it is detected it can be monitored (Liadut 2018).

The alkali-silica reaction has long been a factor that has affected concrete structures over time. It was discovered in 1940 by Stanton (Stanton 1940). Since this time, it has been the subject of many research investigations. However, more recently the number of investigations has increased exponentially as compared to the 20th century. These investigations include determining the cause of the expansion in ASR concrete, understanding the way ASR propagates through concrete, and developing mitigation techniques. Petrography, coring, and visual inspections have typically been the major investigative methods used to research ASR. However, in the most recent decade researchers have also begun to use acoustic emission (AE) to investigate and understand the reaction. Two interesting conclusions made with AE are explained as follows: Farnam et al. (2015) discovered in AE hits with high frequencies (300kHz – 400 kHz) the microcracking begins in the interfacial transition zone, or ITZ, of the aggregate, while in AE hits with low frequencies (100kHz – 300 kHz) the microcracking begins in the ITZ and cement matrix. Abdelrahman et al. (2015) tested concrete prisms under accelerated ASR conditions and found that there was a correlation between the acoustic emission cumulative signal strength and expansion of the prisms. There will be a further discussion on acoustic emission later in this chapter.

This thesis is focused on the relationship between reactivity, aggregate size, and degradation. The effect of aggregate size on the damage distribution of ASR affected concrete has also been investigated using other conventional methods such as mortar bar tests, chemical modelling, and mortar expansion (Payot 2007; Adil 2015; Saouma 2014).

Prior to research surrounding ASR and aggregate size, it was predicted that the ASR expansion would increase as particle size reduced (Stanton 1940; Vivian 1951). However, modern research has seemingly described that as reactive aggregate size decreases there is less of an impact on expansion and degradation as compared to larger reactive aggregates (Multon 2010). Dunant et al. (2012) concluded that in the primary stages of ASR deterioration the expansion's rate depends on the individual aggregate sizes and later stage deterioration depended on the fracture behavior of the cement. Multon et al. (2008) investigated the effects of different aggregate size on mortar bars and concluded that reactive coarse aggregate led to expansion that was seven times larger than reactive fine aggregate expansion. Bazant et al. (1999) suggested that the size of the reactive aggregates has an impact on the swelling pressure of the gel formed during the alkali-silica reaction. While other researchers have proposed different hypotheses to describe the phenomenon observed in the studies, there is clear a link between aggregate size and reactivity. This thesis will provide further insight on this link and will attempt to fill in the gaps of the literature by using acoustic emission, and other non-destructive methods, to understand the differences and similarities of reactive coarse aggregate concrete and reactive fine aggregate concrete.

The effect of reinforcement in a concrete structure is also of interest in this thesis and there is a gap in the literature when it comes to the boundary conditions of concrete and how it affects ASR with different aggregate size, using different non-destructive test methods. Although, the relationship between confinement and ASR has been looked in to. Liaudat et al. (2018) showed that directions with less compression from confinement tend to expand more. Studies at the University of Tennessee and the University of South

Carolina have concluded that the alkali-silica reaction in reinforced concrete leads to expansion along the thickness of the concrete (Soltangharaei 2020). Information surrounding this area of the reaction is relevant because many of the major structures affected by ASR are reinforced, these structures include nuclear power plants and bridges. As discussed above, AE is a top tier method for understanding the damage distribution in concrete, in general, thus making it an efficient method for the condition assessment of ASR effected concrete. The state-of-the-art method of analyzing how multiple non-destructive test methods successfully investigate the relationship between ASR, aggregate size, and boundary conditions will surely further the body of knowledge on the alkali-silica reaction in concrete.

2.1.1 Alkali-Silica Reaction Mechanisms

Although the alkali-silica reaction was discovered in the 1940s, there has only recently been an expansion in the research completed on the subject. The reaction takes a long time (up to multiple decades) to have a major impact on structures, which is the reason for research to only have recently focused on the reaction and its impact. Known structures that have been affected by ASR include the Millennium Stadium in Wales, the Seminoe Dam in Wyoming, The Fairfield Bridge in New Zealand, the Seabrook Nuclear Power Plant in New Hampshire, and many more. There are essentially two solutions to ASR infected concrete. The first is to repair the infected concrete at a high cost, which does not necessarily rid the structure of ASR related gel or cracks. The second option is to simply demolish the ASR infected structure, which also would lead to a high financial burden. Neither of these are a preferred solution for the future, so this thesis will contribute to the state-of-the-art research being completed to develop more beneficial solutions. A

discussion on current mitigation methods as well as the benefit of noticing ASR early are present later in this literature review chapter.

Basic ingredients for the reaction are moisture (usually in the form of humidity), an alkalotic environment, and reactive silica on the aggregate. The basic solution to the ASR problem would be to utilize aggregate that has little-to-no-silica, but this process is not as easy as it sounds (Malvar et al. 2002). The reaction is an acid-base reaction, where the acid is the solid silica and the base is the sodium or potassium hydroxide found in the cement pore mixture. The reaction begins during mixing because of the presence of water. The reaction produces a gel like substance named calcium potassium (or sodium, depending on which alkali is present) silicate hydrate. The alkalis are not actually present during the reaction, it is their hydroxyl ion counterparts that lead to the reaction. In other words, there is silicon dioxide present on the aggregate. The water hydrates the alkali and separates them from their hydroxyl ions. The hydroxyl ions then break the siloxane (silicon dioxide's bonds) bonds, and this is what forms the alkali-silica gel. The gel expands as it is exposed to more moisture and this is what causes the deterioration and expansion in concrete

$$\{Si - O - Si\} + \{R^+ + OH^-\} \rightarrow \{Si - O - R\} + \{H - O - Si\} \qquad \textbf{\textit{(2. 1)}}$$

$$\{H - O - Si\} + \{R^+ + OH^-\} \rightarrow \{Si - O - R\} + \{H_2O\} \qquad \textbf{\textit{(2. 2)}}$$

$$\{Si - O - R\} + \{nH_2O\} \rightarrow \{Si - O^-\} + \{(H_2O)_n\} + \{R^-\} \qquad \textbf{\textit{(2. 3)}}$$
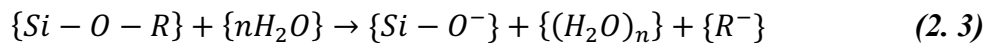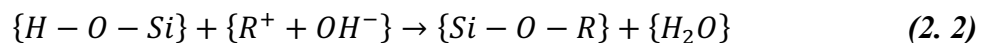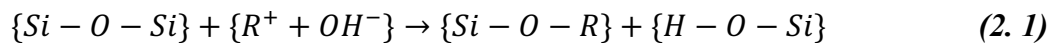
structures. It is important to note that this research takes place over time and it also produces silicic acid (Saouma et al. 2014). See **Equations 2.1 – 2.3** below for a basic depiction.

When the expansion of the gel inside the concrete is not uniform, microcracking begins to occur. The microcracking itself is influenced by the concrete mixture and restraints and the effects can be seen on the surface of the concrete in the form of

10

macrocracks. Overall the major effects of ASR on concrete include microcracks, macrocracks, expansion, induced compressive and tensile stresses, and induced bond stresses between the steel and concrete. A microscopic photo of ASR cracking can be seen below in **Figure 2.2**. Typically, in ASR affected concrete it is common to see the phenomenon known as map cracking. ASR is also incredibly dangerous for structures because it expands slowly and at a rate to which the human eye would not notice. So, as the gel around the aggregates expands and microcracks form, the concrete itself also expands. Even though visual cracks may not be forming, the safety and serviceability of the structure affected by ASR also begins to become compromised.
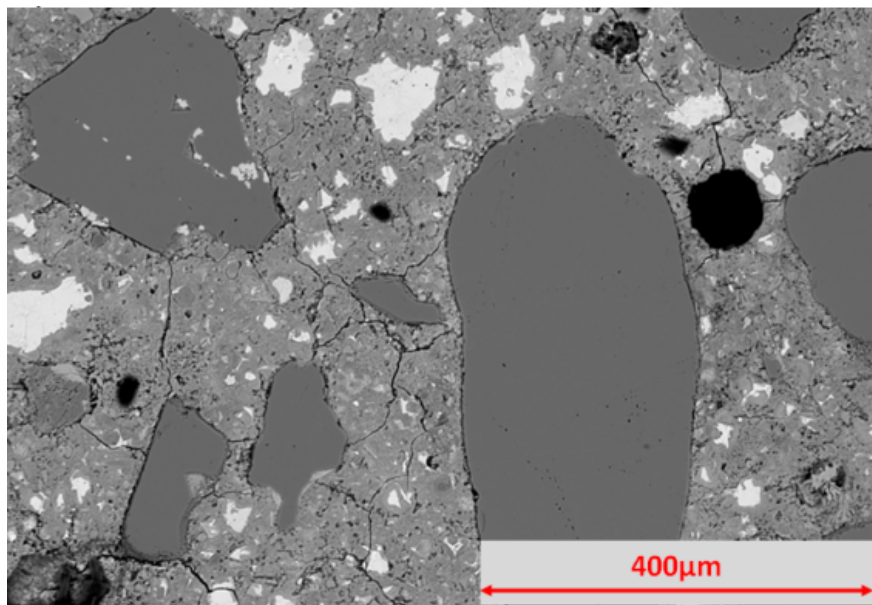
Figure 2.2: *ASR Cracking scanned by electron micrograph (Jozwiak-niedzwiedzka 2018)*

2.1.2 ASR Laboratory Testing Procedures

Listed below are the ASTM standards for testing methods to determine the reactivity of aggregates and the comments about them taken directly from the AAR Fact Book (FHWA):

2.1.2.1 *ASTM C295: "Guide for Petrographic Examination of Aggregates for Concrete":*

11

- Useful evaluation to identify many (but not all) potentially reactive components in aggregates.

- Reliability of examination depends on experience and skill of individual petrographer.

- Results should not be used exclusively to accept or reject aggregate source – findings best used in conjunction with other laboratory tests (e.g., AASHTO T 303 and/or ASTM C 1293).

2.1.2.2 *ASTM C 289: Standard Test Method for Potential Alkali-Silica Reactivity of Aggregates (Chemical Method)*

- Aggregate test in which crushed aggregate is immersed in 1M NaOH solution for 24 hours – solution is then analyzed for amount of dissolved silica and alkalinity.

- Poor reliability.

- Test is overly severe, leading aggregates with good field performance to fail the test.

- Some reactive phases may be lost during pretest processing.

2.1.2.3 *ASTM C 227: Standard Test Method for Potential Alkali Reactivity of Cement-Aggregate Combinations (Mortar-Bar Method)*

- Mortar bar test (aggregate/cement = 2.25), intended to study cement-aggregate combinations.

- Specimens stored in high-humidity containers at 38°C.

- Several reported problems with test, including excessive leaching of alkalis from specimens.

2.1.3: ASR Mitigation

As discussed above, it is evident there are four main components that lead to the alkali-silica reaction. The components are reactive silicas found in aggregates, alkalis (mainly the hydroxides attached to the alkalis) commonly found in cement, soluble Ca, and a humid environment or any environment that provides moisture to allow for expansion of the silicate gel (Rajabipour 2015). Rajibipour et al. (2015) elaborates on most of the known mitigation efforts in use and the pros and cons with each of them.

There are more options for new construction to prevent, or mitigate, the reaction from occurring as compared to mitigating existing structures that are experiencing ASR related damage. These options begin with what seems to be the simplest choice, which is to simply only use aggregates with a very small likelihood of being reactive. However, as already discussed in this chapter, there is a lot of uncertainty surrounding selecting aggregates with low reactivities. Additionally, there is not a large supply of aggregates with low levels of reactivity. Another mitigation strategy for new construction is to follow AASHTO-PP65 and limit the alkali content in the concrete solution. The standard calls for a maximum alkali content of $1.8 \ kg/m^3$ (AASHTO-PP65 2013). There are standards available to reduce the amount of reactions occurring in new concrete, however, the standards have not always been reliable. An additional mitigation strategy is to avoid using cement in the concrete mixes. This easily reduces the amount of alkalis that will be present in the pore solution, but this will yield in concrete that does not have equivalent properties to Portland cement concrete. These properties include freeze-thaw scaling, strength development, and setting. Although this is currently the most common way to avoid ASR for new construction, there is a limited availability of supplementary cementitious material (Rajabipour 2015). Lastly, new construction can opt to add certain admixtures to concrete

13

in order to add compounds or chemicals that reduce the effectiveness of the reaction. Lithium has been shown to have this effect (Kawamura 2003; Mo 2005). Although, the chemical is not widely available, additives like this chemical would be great for the future of mitigation of ASR.

As discussed previously, there are fewer options for engineers when it comes to existing construction as opposed to new construction. ASR propagates from the inside of concrete towards the outside, which is why there is difficulty mitigating it in existing structures. Accessing the source of the reaction becomes increasingly more difficult in structures as the thickness of the structures increase; this is especially a problem in structures with a very large concrete thickness, like nuclear power plants. Aside from this problem, the surfaces of the affected concrete can still be accessed and there are a few mitigation methods widely used to repair structures. Treatment of the surfaces with Lithium via electromagnetic or vacuum impregnation, or topical application, have had success in treating surface ASR (Rajibpour 2015). Other mitigation methods include crack filling, encasing the structure with new concrete, and slot cutting. However, these methods are like putting a band-aid on an abrasion that needs stiches, because they are simply solving immediate symptoms, not the overarching problem of ASR (Rajibpour 2015). Although, the mitigation method that has seen the most effective results is to reduce the exposure to moisture by improved drainage or sealants (Fournier 2015).

The methods discussed in this section are most effective when ASR is detected early. Take two identical water treatment structures that are affected by ASR, the first structure's, structure A, ASR problem is detected early, while structure B's ASR problem is only noticed by the time visual map cracking begins to appear. Structure A is likely to

have a much longer serviceability lifetime because solutions like improved drainage can be implemented in areas where high moisture exists. In addition, monitoring early stage ASR will lead to a better understanding of how reliable and serviceable any affected structure is at any given time. Noticing expansions and crack growth can save lives, so it is always best to detect ASR as soon as possible. The FHWA conducted a few field tests and one of their major takeaways when dealing with ASR was to "start monitoring as soon as possible." The data accrued from field monitoring will also eventually assist in finding a long-term solution to the problem. (Thomas 2013)

2.2: Acoustic Emission

In the fields of civil and structural engineering, Acoustic Emission (AE) has recently been a useful technique to assess the condition of concrete structures. The anomaly known as AE is the release of acoustic, or elastic, waves inside mediums, such as concrete. The waves are formed by the release of energy, and in concrete structures this
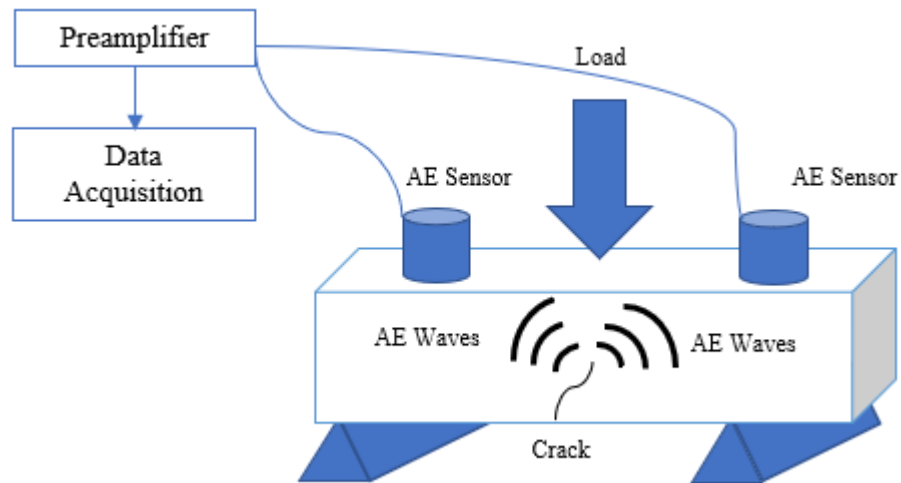

Figure 2.3: Acoustic Emission Setup (Modeled after Soltangharaei 2018)

energy release usually results from crack formations or crack growth (ASTM E1316). The waves travel through the concrete towards the surface, which is where the AE sensors are typically placed. Although, some literature has used AE sensors embedded inside concrete

(Soltangharaei 2018). AE is a form of non-destructive testing and this is because the sensors simply monitor the damage being experienced; they do not require material damage in order to begin a test. Other common ways to test concrete, like petrography and coring, are destructive test methods because the methods require the material/concrete to be destructed. So, in many applications where structures cannot be disturbed, such as nuclear facilities and prestressed concrete applications, AE is an efficient data acquisition replacement to common methods. Commonly, piezoelectric sensors (made from lead zirconate titanate, or PZT, ceramic) are used to acquire AE data. The sensors can detect very small releases of energy inside concrete, which makes AE such a useful technique. AE does require a large amount of data filtration because the sensors are so sensitive (within the ultrasonic frequency range) and can detect very small disturbances, however. The methods used in this study for data filtration are further addressed in **Chapter 3.** The sensors convert the energy release into electric signals for analysis. See **Figure 2.3** for a depiction on how AE sensors are typically laid out on a concrete specimen during a three-point bending test. AE allows for real-time data to be collected at a range of different time scales; it is suitable for long-term and short-term acquisition. AE also allows for data to be collected without excitations or loads being applied to a specimen. The passive ability of this type of testing makes it such a great choice when analyzing the effects of ASR.

There are two main types of piezoelectric sensors that are used in research: broadband, or wideband, sensors and resonant sensors. There are pros and cons to each type. Resonant sensors are much more sensitive than broadband sensors but are only this sensitive at its resonant frequency. The broadband sensors can sense a range of different frequencies, but the sensitivity is not as high as compared to the resonant sensors.

16

Broadband sensors are of better use when the frequency being analyzed is unknown, whereas resonant sensors are better when there are more features that are of interest, including amplitude and energy. When deciding on a resonant sensor it is imperative to select the correct frequency range. Although, there are positives to using one sensor over the other, it is not uncommon for researchers to use both types when conducting experiments.

Typically, in the past, AE has been utilized for data acquisition in concrete load testing as well as the monitoring of concrete embedded with corrosive steel (Abdelrahman 2015; Ono 2011; El Batanouny 2014; Ziehl 2016). Other popular uses of AE monitoring in the fields of civil and structural engineering include bridge and beam assessment (Yu 2011; Anay 2016), and in concrete structures affected by the alkali-silica reaction (Abdelrahman et al. 2015). Additionally, many methods such as coring, mechanical strain gauges, crack indexing, visual inspection, petrographic analysis, and more have been used to assess the damage distribution of ASR concrete (Thomas et al. 2013). The methods mentioned are adequate but have their deficiencies in comparison to AE. For example, AE detection methods allows for microcracks to be found, while visual inspection of concrete can only be used when cracks form on the surface of concrete. Therefore, AE is more satisfactory in detecting early signs of ASR. Early crack detection is of greatest importance in concrete applications where there is a thick layer of concrete, such as nuclear containment facilities or dams, in question. AE is also a better option than many other common testing methods because it is less time consuming and less dependent on the individual conducting tests. Visual inspection can be a subjective method at times, but even with the advancement in drone inspection technology AE remains superior. Strain gauges

17

are suitable for piles, beams, and columns, but are not as useful when studying shear walls. This is because shear expansion can happen through the thickness of the wall as compared to the surface of the wall, which is where a strain gauge would be placed. Crack indexing is a localized monitoring technique and is not determinant of an entire structure. Indexing also takes a while to complete compared to the time that it takes to set up the AE system. Coring is a method that cannot be used in certain applications because it is a destructive method that requires multiple samples, and even with the multiple samples it is still not simple to determine the condition of a full structure from the few samples taken.

The civil engineering research industry has made many strides in classifying, modelling, and understanding the deleterious reaction that is the alkali-silica reaction, over the last decade. Firstly, important components in the reaction are the aggregates composition and mineralogy. Rajabipour et. al (2015) noted that certain natural silicates are more susceptible to ASR; these silicates include opal, cristobalite, and trydimite. Another important mechanic in the reaction is the aggregate size, which has been addressed in this literature review.

2.2.1 Acoustic Emission Terms/Parameters

The waves generated during acoustic emission testing have many properties that can be analyzed. ASTM E1316 "Standard Terminology for Nondestructive Examinations" defines many of these terms related to acoustic emission during data acquisition for damage, and the definitions for the most relevant ones to this study, as well as parameters that can be calculated and analyzed, are listed below:

- **Acoustic Emission:** "The class of phenomena whereby transient elastic waves are generated by the rapid release of energy from localized sources within a material, or the transient waves so generated" (ASTM E1316).

18

- **Amplitude:** "The peak voltage of the largest excursion attained by the signal waveform from an emission event" (ASTM E1316). See **Figure 2.5** for a depiction.

- **Duration:** "the time between AE signal start and AE signal end" (ASTM E1316). See **Figure 2** for a depiction.

- **Energy:** "the energy contained in a detected acoustic emission burst signal, with units usually reported in joules and values which can be expressed in logarithmic form (dB, decibels)" (ASTM E1316).

- **Event:** "a local material change giving rise to acoustic emission" (ASTM E1316).

- **Hit:** "the detection and measurement of an AE signal on a channel" (ASTM E1316).

- **Rise Time:** "the time between AE signal start and the peak amplitude of that AE signal." (ASTM E1316). See **Figure 2.3** for a depiction.
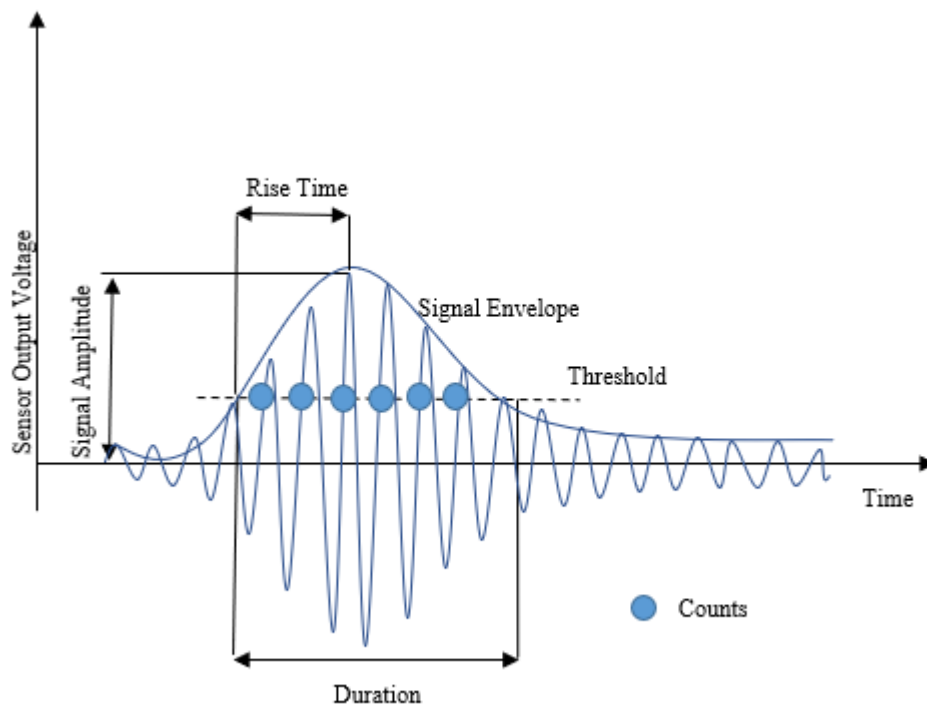
Figure 2.4: *Acoustic Emission Waveform (Modeled after Soltangharaei 2018)*

- **Count:** "the number of times the acoustic emission signal exceeds a preset threshold during any selected portion of a test" (ASTM E1316).

- **Signal Strength:** As defined by the Physical Acoustic Corporation, or PAC, "signal strength is defined as the integral of the rectified voltage signal over the duration of the AE waveform packet. It is sometimes referred to as relative energy which relates to the energy amount released by the material or structure" (Nor et al. 2011). In this study it will typically be measured in picovolts (pVs).

- **Threshold:** "a voltage level on an electronic comparator such that signals with amplitudes larger than this level will be recognized. The voltage threshold may be user adjustable, fixed, or automatic floating. (E 750)" (ASTM E1316).

- **Hit Definition Time (HDT):** "This parameter specifies the maximum time between threshold crossing, i.e. if no crossing occurs during this time then the hit has ended. If the HDT is set too high then the system may consider two or more hits as one. If the HDT is set too low then the system may not fully capture the AE hit and possibly treat one hit as multiple ones" (Rúnar 2013).

- **Historic Index:** The historic index is a metric that measures the change in cumulative signal strength (CSS) over a given duration for a test, or the slope of the CSS vs time graph.

- **Hit Lockout Time (HLT):** "This parameter specifies time which must pass after an hit has been detected before a new hit can be detected. If the HLT is set too high then the system may not capture the next AE and if it is set too low then the system may capture reflections and late arriving component of the AE as hits" (Rúnar 2013).

- **Severity:** The severity of any given amount of data can be determined with an intensity analysis after gathering an understanding of the historic index. It is essentially the average signal strength of a given data set having the maximum signal strength value (Jones 2012).

- **Peak Definition Time:** "parameter specifies the time allowed, after a hit has been detected, to determine the peak value. If the PDT is set too high then false measurements of peak value are more likely to occur. It is recommended that the PDT should be set as low as possible" (Rúnar 2013).

2.2.2: AE Filtering/Analysis Methods

As seen above, there is a multitude of information that comes along with acoustic emission data acquisition. Researchers must know what to look for and sort out noise from meaningful data. Literature related to acoustic emission presents a few ways to filter data as well as analyze data. A common method used in data filtering is known as duration-amplitude filtering and it stems from the consensus that acoustic emission hits with a low amplitude and a high-rise time are typically noise hits and not meaningful (Tinkey 2002). These are also known as Swansong II filters. Acoustic emission tests with a relation to concrete are apparent in the literature using this filtering method, as well as methods like the R-A filtering method that is very similar (Anay 2016). The specific filtering methods used in this thesis are addressed in **Chapter 3.**

Subsequently, after filtering the data it should be ready for analysis. The parameters that are acquired from acoustic emission data acquisition can lead to very effective analysis. The primary AE parameters used in this study are signal strength and cumulative signal strength (CSS). Signal strength's definition can be seen in the section above, and the cumulative signal strength is the summation of signal strengths over a certain time period.

In analysis, it is typical to plot CSS versus time. These plots will lead to an efficient explanation of when damage occurred inside the specimen in question over that time period. Higher rates of increased CSS are strong indicators of damage, microcracking, and/or expansion. The effectiveness of this metric has been evaluated in many research investigations including composite (Kumar 2017), concrete testing (Elbatanouny 2014 & Elbatanouny 2019), and even in the analysis of ASR affected concrete (Soltangharaei 2020). The rate at which the CSS changes over time is closely linked to the next parameter discussed in this thesis: historic index.

The historic index is also defined above in the parameter section. This parameter can play a very pivotal role in acoustic emission data analysis, as it uniquely describes major changes in the CSS. It also can assist in determining an intensity analysis, which will be discussed later in this section. The equation to find historic index is expressed in **Equation 2.4**.

$$H(t) = \frac{\sum_{i=K+1}^{N} S_{Oi}/(N-K)}{\sum_{i=i}^{N} S_{Oi}/N} \qquad (2.4)$$

$$with \; K = \begin{cases} 0 & N < 200 \\ 0.8N & 200 \le N \le 1000 \\ N - 200 & N \ge 2000 \end{cases}$$

In **Equation 2.4** N is the number of hits up to time *t*; S_{Oi}= signal strength of the *i*th hit; and K = empirically derived factor that varies with the number of hits and material type (Benedetti 2014). This parameter is incredibly effective because there is no limitation based on specimen size and the historic index can detect damage onset in a variety of conditions. The historic index can also be plotted with the severity index to form an intensity plot. The

severity index is also defined in the parameters above and can be calculated with **Equation 2.5.**

$$S_r = \frac{1}{J}(\sum_{M=1}^{J} S_{Om} \qquad\qquad (2.\,5)$$

In **Equation 2.5**, S_r represents severity, J represents empirically derived constants based on certain mediums or materials, and S_{Om} represents the signal strength of the *m*th hit (Shahidan 2013). A plot of the historic index maximum and severity index represents the intensity of the data being analyzed. The chart can be separated into sections where the top right most points represent the most intense information, while the bottom left represents the least intense information. In the context of this thesis, a point in the lower left would represent ASR being less active in a certain specimen; the opposite would be true for a point in the upper right of the chart.

2.2.3: Challenges with Acoustic Emission

Although the use of acoustic emission for non-destructive monitoring has experienced an exponential increase in activity over the last decade, there are still many challenges that present themselves while dealing with acoustic emission data. Primarily, there are a multitude of piezoelectric sensors that data collectors can choose from, and each type of sensor has their own pros and cons. For example, wideband sensors will collect less data at a larger range than broadband sensors. However, broadband sensors will collect more data in a more centralized area as opposed to broadband sensors. This becomes challenging in research because each senor location is unique and may not encounter the same amount of damage as another location. It is important when using acoustic emission sensors to use a variety of sensor types when testing in order to account for all the variations of damage than could occur throughout a specimen. Additionally, not all research projects are funded equally, and these sensors can range from a few hundred dollars to thousands

of dollars. Ideally, researchers would use the most sensitive and most resistant to noise, but there are other ways to avoid these challenges other than a higher budget.

Noise is a recurring problem that researchers using acoustic emission often must face. In this thesis, noise is data encountered that does not have a meaningful impact. Noise can be encountered in many ways, including subtle vibrations via walking, a door opening and closing, water dripping and making a sound, or even noise that cannot be detected by human's ears. It is evident from the literature that different types of damage release damage in different ways. This can be seen from simple acoustic emission features like frequency, or more detailed characteristics like FFT's of each hit. For example, Farnam et al. (also discussed earlier in this chapter) explained that different types of microcracking occur at different frequencies (Farnam 2015). Additionally, Zhang et al. explained that when monitoring energy and frequency for rock rupturing, a high frequency but low energy signal is apparent in small-scale cracking, but the opposite is true regarding large-scale cracking (Zhang 2018). Clearly, it is important to monitor these parameters for ASR testing. However, the existence of noise can hinder results like the ones discussed above. So, in this thesis the author used a method of creating an amplitude floor during data collection to reduce the noise signals. The author also used a filtering system once all the data was collected to ensure that all data being analyzed had meaning. **Chapter 3: Experimental Setup** will discuss these two methods in more detail.

2.3: Additional Analysis Methods

The results presented in this thesis use AE and other non-destructive methods to analyze the ASR data presented**.** The primary purpose of this thesis is to investigate different evaluation methods and understand the correlation between aggregate size, boundary condition, and ASR activity. An additional parameter that is used to understand

24

ASR in concrete related structures is strain. Expansion is present in any concrete structure affected by ASR and it is one of the most critical products of the reaction. However, it also is one of the most helpful parameters that a researcher can observe. Expansion is a critical component of ASR, and a lot of literature surrounding ASR involves monitoring strain and expansion, see Soltangharaei et al. (2018), Morenon et al. (2017), Jones et al. (2013), and many more.

In addition to expansion and acoustic emission, this thesis also presents progressive pictures and measurements of crack growth. Understanding how large cracks are becoming as well as the rate at which the cracks grow can yield meaningful results when it comes to concrete structures. Crack patterns, growth rates, microcrack formations, and different types of cracking under varied loading tell engineers important information about structures. Concrete's brittle nature also increases the importance of monitoring cracks as soon as possible. Hillerborg et al. (2013) elaborates on the importance of monitoring cracks and how monitoring cracks helped him discover the relationship between bending strength and tensile strength. Monitoring cracks related to concrete is important; however, there is not much research that expand on the formation and growth of cracks when it comes to ASR. It is widely known that ASR leads to map cracking, expansion, and the degrading of structures; therefore, there may be a correlation between crack growth and ASR. Teramoto et al. (2018) used a digital image technique to monitor the formation and growth of microcracks related to ASR, and he concluded that mechanical properties of aggregates used in the formation of concrete directly affect the crack growth of ASR cracks.

Crack formation and growth affects the function of concrete as well as the interior make-up. A typical way to measure how the inside of any material has been affected by

cracking, or any other type of degradation, is by an ultrasonic pulse velocity test, or UPV. A UPV test is non-destructive and is an attractive method for monitoring a variety of tests on concrete. A UPV test sends waves through one side of the concrete to the other and it can measure how fast the waves travel, how far the waves had to travel, and many different parameters. Hobbs et al. (2007) noted that UPV was helpful in determining the strength differences in varied types of concrete. Measuring how fast waves travel through concrete is important because if UPV tests are done throughout the life of concrete the waves are slowly going to travel the same distance at a slower pace because there is more interior degradation preventing the waves from travelling as fast as they would inside pristine concrete. This is certainly of interest in ASR related damage because understanding how different aggregates and boundary conditions effect concrete from the inside would provide more insight towards a correlation between aggregate size, boundary conditions, and damage.

Each evaluation method described above has its pros and cons. For example, acoustic emission is incredibly sensitive and can detect small cracks, but a lot of noise can come from it. Crack growth measurements are only possible once cracks have begun to show, so it is difficult to analyze early in the ASR process. UPV waves travel at a low frequency (as compared to AE waves), so it is likely that microcracks can be missed. This thesis focuses on mitigating the problems encountered by these testing methods and investigating them to determine the effectiveness of each when analyzing ASR affected concrete.

CHAPTER 3

Experimental Setup

3: Experimental Setup Introduction

The setup for this whole study consists of two separate tests that were run one after the other. The major difference between the tests is in the concrete's composition, while the testing procedure and setup remained the same throughout both tests. This chapter is broken up into two sperate subchapters. The first will explain the preparation of the specimens, while the second will explain the test's setup and instrumentation.

3.1: Specimen Preparation

Each test setup consisted of three concrete specimens, of which two were composed of the reactive coarse, or fine, aggregate and the third was a control specimen. The coarse specimens were procured at the University of Alabama and moved to the University of South Carolina to be placed in the high humidity/temperature chamber. The reactive fine aggregate specimens were procured at the University of Nebraska. The dimensions were 12 in x 12in x 44 in. One reactive specimen was fitted with rebar along the X and Z axes, this specimen is denoted as the "confined" specimen, while the reactive specimen without reinforcement is denoted as the "unconfined" specimen. The figures and tables displayed in this chapter are taken from the NEUP Project 16-10214 proposal because the author did not have access to the specimens prior to their creation.

There were four aggregates used in the creation of the concrete specimens. **Table 3.1** shows the location from where each aggregate came from, the specific gravity (SSD), the absorption percentage, and DRUW of each aggregate. **Figure 3.1** is a gradation plot for each aggregate as well.

Table 3.1: *Aggregate Information (Malone 2019)*

	Location	Specific Gravity (SSD)	Absorption	DRUW (lb/ft³)
Non-Reactive Coarse	Omaha, NE	2.617	2.57%	103.97
Non-Reactive Fine	Omaha, NE	2.651	0.42%	-
Reactive Coarse	Gold Hill, NC	2.722	0.039%	92.42
Reactive Fine	Robstown, TX	2.658	0.70%	-
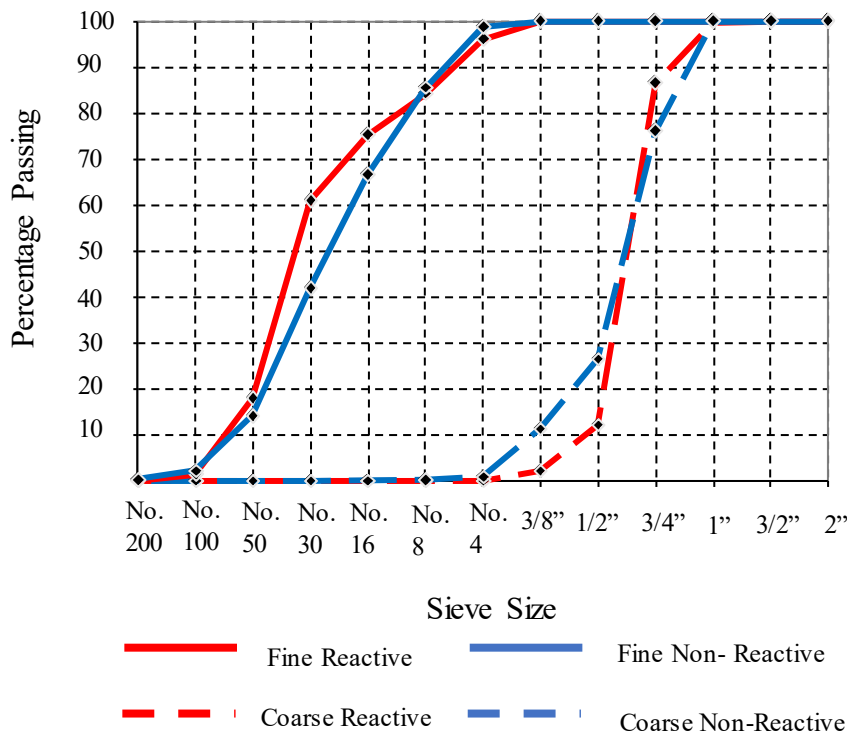
Figure 3.1: *Gradation of Aggregates (Malone 2019)*

The cement used in the concrete was ASTM C150 (2018) Type I/II Portland

Cement. See **Table 3.2** for a chemical composition of the cement. In order to impact the

flowability of the concrete a polycarbonate based HRWR was used as an admixture at 3-

12 fl oz/cwt.

Table 3.2: *Cement Information (Malone 2019)*

Chemical Properties	Oxide (%)	SiO_2	20.4
		Al_2O_3	4.1
		Fe_2O_3	3.1
		CaO	63.8
		MgO	2.3
		SO_3	2.7
	Na_2O_{cq}		0.47
	Loss on Ignition		2.5
Physical Properties	Blaine Fineness (m^2/kg)		443
	Specific Gravity		3.15
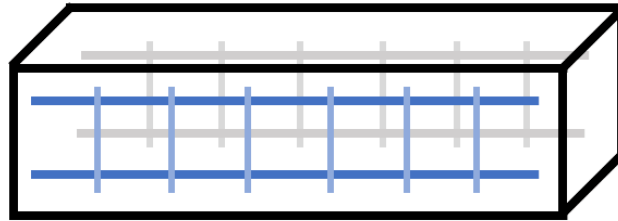
Figure 3.2: *2D Reinforcement Plan (Malone 2019)*

Figure 3.3: *Rebar Placement Prior to Casting (Malone 2019)*

The concrete was cast inside a wooden framework that satisfied the dimensions and ensured a smooth exterior. The confined specimens were reinforced with grade 60 headed rebar. The longitudinal directions were fitted with four 40-inch-long #7 bars, and the
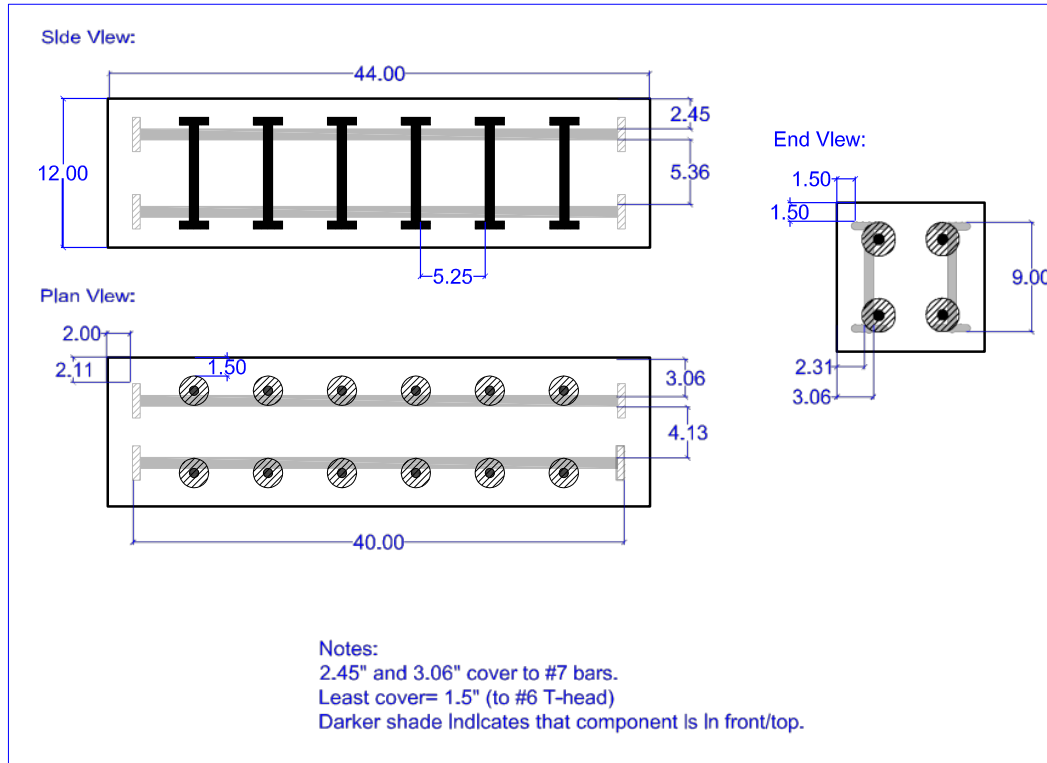
Figure 3.4: *2-D Reinforcement of Specimens (Malone 2019)*

vertical directions were fit with twelve 9-inch-long #6 bars. Cable ties were used to connect

the rebar, and **Figure 3.2** – **Figure 3.4** describe the reinforcement plan.

The mix design for the concretes can be seen in **Table 3.3**. The control mixes used

innocuous aggregate and low-alkali cement. The reactive mixes consisted of innocuous and

reactive aggregates depending on the specimen being procured. In the reactive specimens,

an alkali booster was used to accelerate the reaction.

Table 3.3*: Theoretical Mix Design (SSD) (Malone 2019)*

Component	Control	Reactive Coarse Aggregate	Reactive Fine Aggregate
	Weight (lb/yd^3)	Weight (lb/yd^3)	Weight (lb/yd^3)
Cement	590	590	590
Water	295	295	295
Coarse Aggregate	1900	1751	1846
Fine Aggregate	1195	1415	1252
HRWR	4.0 oz/cwt	4.0 oz/cwt	4.0 oz/cwt
50/50 NaOH, lb	0	15.69	15.69
w/c	0.5	0.5	0.5

31

3.2: Test Setup and Instrumentation:

After the specimens were received by the University of South Carolina, sensors were attached to each specimen prior to being placed in the chamber. Ten sensors were epoxied onto the surface of each reactive specimens, and four sensors were placed on the surface of the control specimens. The sensor locations are tabled in **Table 3.4** and depicted in **Figure 3.5**. All sensors used were PKWDi with 26-dB preamplification. The testing chamber is in the structures/geotechnical laboratory at the University of South Carolina. It is an 8' x 8' x 4' container made from plexiglass.

Table 3.4: Sensor Locations

Sensor No.	Reactive Specimens			Control Specimens		
	X (in)	Y (in)	Z (in)	X (in)	Y (in)	Z (in)
1	110	90	0	110	120	90
2	330	30	0	330	120	30
3	110	30	120	110	0	30
4	330	90	120	330	0	90
5	110	120	90	-	-	-
6	190	120	30	-	-	-
7	330	120	30	-	-	-
8	110	0	30	-	-	-
9	250	0	90	-	-	-
10	330	0	90	-	-	-

To reduce error within the chamber the sensor-to-cable connection was moisture protected with heat shrink tubing. During testing hours, the chamber remained at 95% ± 5% relative humidity and at 37 ± 3 degrees Celsius. A humidifier and a heater keep the chamber at these levels, and the humidifier distributed moisture evenly throughout the chamber. Chamber maintenance as well as strain measurements and data acquisition were the only reasons testing and data collection were halted. Chamber maintenance included simple cleaning, monitoring the temperature and humidity, and pencil lead breaks to ensure the data acquisition system was working properly. To ease access in and out of the chamber

the specimens were fitted onto rolling steel carriers and the bottoms of the specimens were protected by neoprene pads to reduce noise from the ground and potential vibrations.

Each month strain measurements were taken using DEMEC gauges (demountable

a) Control Specimen

b) Reactive Specimen
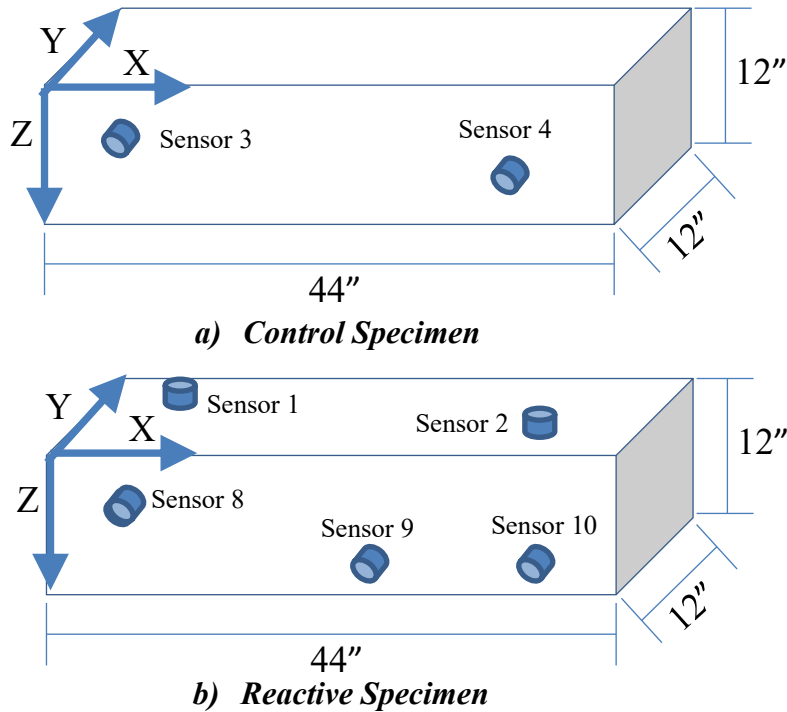
Figure 3.5: *Sensor Locations Depicted (Not to Scale)*

mechanical strain gauges) with lengths of 20 in. in the X-direction and 6 in. in the Y and Z direction. In addition to strain measurements, each month (once cracks appeared) a Dino-Lite digital microscope was used for crack measurement and to take microscopic images ranging from 210 to 220 times resolution. The inspection procedure included precise visual inspection for minor surface cracks. The data acquisition machine used was a 24 channel (10 confined, 10 unconfined, and 4 control) Micro-II Express, manufactured by MISTRAS Group, Inc. (Princeton Junction, NJ, USA). The sampling rate of this machine is 5 million samples per second, and the settings used can be seen in **Table 3.5**.

Table 3.5: *Data Acquisition Setting*

Setting	Value
Sampling Rate	5000 kHz
Threshold	32 dB
Pre-trigger Time	256 μs
Hit Definition Time	400 μs
Peak Definition Time	200 μs
Hit Lockout Time	200 μs
Low-Pass Digital Filter	400 kHz
High-Pass Digital Filter	20 kHz

Data was collected for 300 days and analyzed using the AEWIN software. As discussed in the literature review chapter, acoustic emission can yield a lot of noise, or meaningless data. A filtering method was used in which the data points were only accepted if a single event was detected by a certain number of sensors. This number was at least four sensors for reactive specimen hits and 2, or 3, sensors for control specimen hits. The data was filtered using MATLAB and analyzed further using Microsoft Excel. Excel was also used in analyzing the UPV, crack growth, and strain data gathered during different times throughout the test. **Figure 3.6** shows the control specimen located in the chamber prior to testing.

Figure 3.6: *Control Specimen inside Chamber*

CHAPTER 4

Results and Discussions

4.1: Introduction

The major discussions and comparisons presented in this chapter include a strain comparison, general acoustic emission parameters, a UPV comparison, and finally a comparison on crack growth. The coarse concrete data, as described in **Chapter 3** comes from a accepted paper by the author's colleague titled "Temporal Evaluation of ASR Cracking in Concrete Specimens Using Acoustic Emission" (Soltangharaei 2020). The author was given the results of this test to compare to the results of the subsequent fine concrete results. The findings and discussion are presented in this analysis chapter of the thesis.

Another objective of this thesis is to investigate different evaluation methods for understanding ASR degradation. This can be analyzed by comparing the reactive specimen data at the final step of each test with the control data at the same points. Contrasting these data sets can show the effectiveness of each evaluation method because the control specimens can represent concrete structures at the beginning of their use. Differences between the control and reactive specimens outline the usefulness that each method brings to the table and show how effective each method was at collecting data for early stages of ASR. So, at the end of each subsection in this chapter, a section contrasting the control results to the reactive results to outline the effectiveness of each measurement used is discussed.

In total there are 6 concrete specimens that will be addressed in this chapter. This includes a confined coarse, unconfined coarse, coarse control, confined fine, unconfined fine, and fine control. Note that throughout this thesis the data presented in red represents the confined reactive coarse aggregate specimen, the data presented in blue represents the unconfined reactive coarse aggregate, the data presented in green represents the confined

37

reactive fine aggregate, and the data presented in pink represents the unconfined fine reactive aggregate.

The three coarse specimens were kept in the humidity chamber together, subsequently, the three fine specimens were also kept in the humidity chamber together. The coarse specimens were monitored for nearly two years and the fine specimens were monitored for nearly 8 months after the coarse specimens were taken out of the chamber. In order to conclude on information about these specimens it is important to mention that the data that will relate the two types of concrete is not based on how long the specimens were in the chamber but is based on similar strain expansions. See **Figure 4.1** for the visual strain comparison, which is discussed in the following section of this chapter.
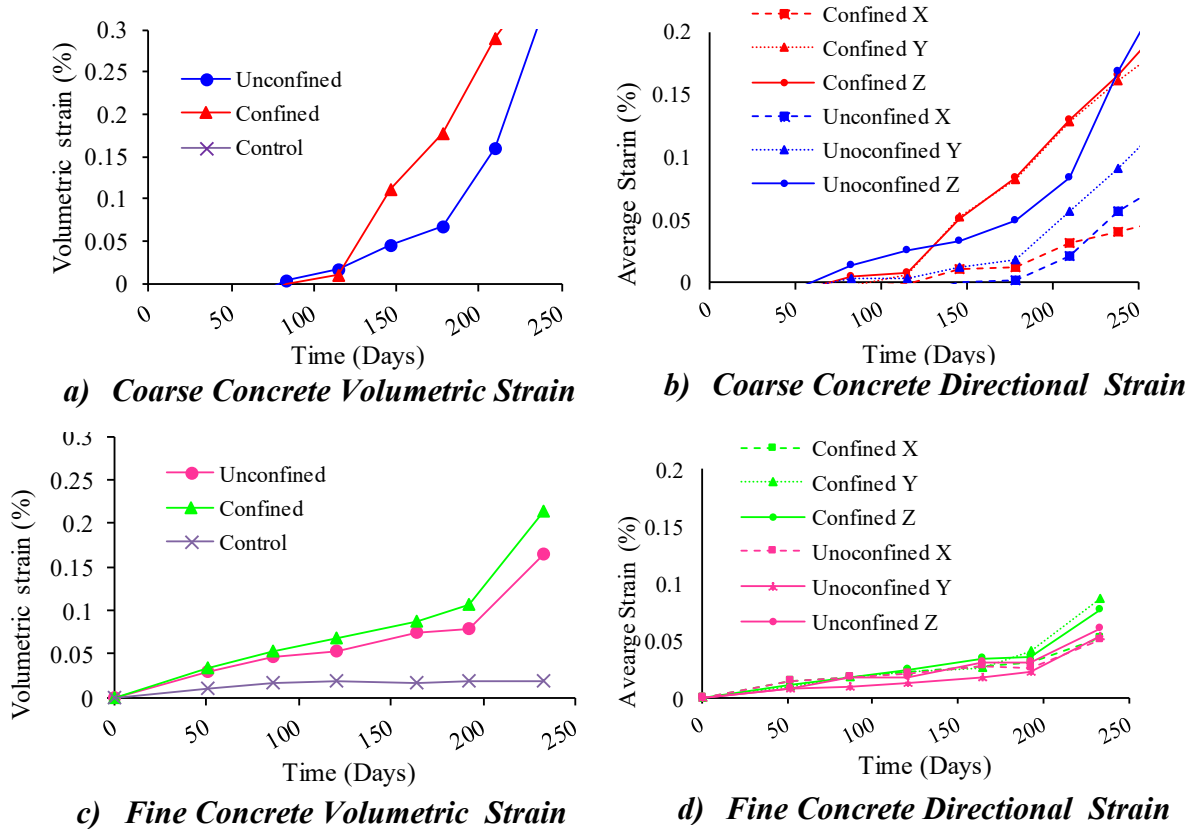

a) **Coarse Concrete Volumetric Strain**

b) **Coarse Concrete Directional Strain**

c) **Fine Concrete Volumetric Strain**

d) **Fine Concrete Directional Strain**

Figure 4.1: *Strain through 250 Days*

4.2: Strain

Generally, in both completed tests, the reactive specimens expanded while the control specimen did not experience the same expansion. This expansion is apparent in concrete structures that are affected by the ASR reaction, so the control specimen's expansion should be low in comparison to the reactive specimens. The control specimen for the reactive coarse aggregate concrete experienced some shrinkage. The control specimen in the reactive fine aggregate concrete test did show some initial expansion, but the expansion did not continue the active days continued. The expansion over the duration of the entire test is nearly zero, so the results are still meaningful and provide evidence to support this thesis. The directions shown in the figures are explained as follows: The X direction is the length of the concrete, the Y direction is the width of the concrete, and the Z direction is the depth of the concrete. See **Figure 3.1** in the previous chapter for a depiction of the directions.

4.2.1: Reactive Fine Specimens

The average strains in all directions of the reactive fine concrete specimens increase at relatively close rates, and the confined Y and Z directions, as well as the unconfined Z direction, lead the way. The Z direction is the direction that is parallel to the casting direction, and Smaoui et al. (2014) noted that this direction is prone to a lower tensile strength. The unconfined specimen's largest directional strain is in the Z, but the confined specimen's largest is the Y direction. Clearly, confinement plays an important roll in directional expansion. The confined specimen also has higher strains in general, which also is what leads to its larger volumetric strain. The confined specimen's Z and Y directional expansions are very similar. Like above, the large Z direction expansion can be attributed to the casting direction. In comparison to the confined specimen's X direction, the Y

expansion is larger than the difference in the unconfined specimen. This can be attributed to the data acquisition method and the strain gauges used. Since the depth (Z) direction of the concrete is reinforced with steel it is likely that there was a redistribution in the ASR stresses that led to this increase in the width.

The unconfined fine specimen seems to expand in an isotropic manner, and the confined fine specimen expands in a slightly more anisotropic manner than the unconfined because of the X direction's smaller strain.

4.2.2: Reactive Coarse Specimens:

As described in **Chapter 3**, the reactive coarse aggregate specimen's data are the results of testing completed prior to the author's research. In addition to this chapter, the results can also be seen in the author's colleague's, Vafa Soltangharaei, dissertation (2020) called "Evaluation of Temporal Damage Progression in Concrete Structures Affected by ASR Using Data-driven Methods." In order to provide a relevant comparison between the fine and coarse specimens it is important to discuss results provided by Soltangharaei et al. (2020).

The volumetric strain for the unconfined coarse specimen is smaller than the volumetric strain for the confined coarse specimen. However, as shown in **Figure 4.1b**, the strain in the unconfined Z direction is increasing at a rate that is comparable to the Y and Z direction of the confined specimen. Smaoui et al. (2014) also explained that aggregates with more surface area produce more expansive gel, and the expansion of ASR gel is what leads to microcracks and damage. If the larger and flatter aggregates are consolidated parallel to the casting direction, then it is likely that the depth (Z) direction will yield a larger, or more rapid, expansion (Smaoui 2014). The other directions in the

unconfined specimen are the two lowest averages, so it is expected that there will be the least degradation/cracks in this direction.

4.2.3: Strain Comparison

It is important to note that the coarse specimens were kept in the humidity chamber for a longer time that the fine specimens. In **Figure 4.1a** there is data that surpasses the entire duration of **Figure 4.1c**. In order to make an accurate comparison between the two tests, and to eliminate error, it is necessary to convert total days into a compatible time period. During each of the tests, the specimens were measured, and chamber maintenance was completed nearly every month. Therefore, the days shown in **Figure 4.1** are not necessarily all days in which the specimens were subjected to high humidity. The periods in which the specimens were subjected to high humidity will hereinafter be recognized as "active days." To solve this problem, the specimens will be compared using active days and similar strains because with these parameters, an accurate conclusion can be made. In **Figure 4.1**, at 210 days, the unconfined coarse specimen's volumetric strain is .16%, while the confined coarse specimen's volumetric strain is .29%. Also, the confined fine specimen's last volumetric strain measurement is .21%, while the fine unconfined specimen's last volumetric strain measurement is .16%. Above is **Figure 4.2** that shows
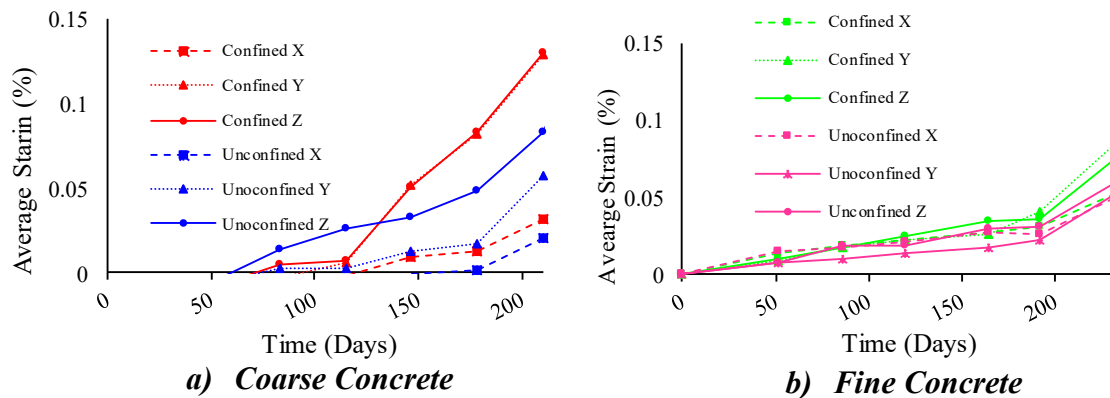

a) Coarse Concrete   *b) Fine Concrete*

Figure 4.2: *Average Directional Strains through Adjusted Days*

41

the coarse specimen's average directional strain up to 210 days and the fine specimen's average strains up until its final measurement. Through active day manipulation, 210 days of coarse testing is equivalent to 233 days of fine testing.

Noticeably, in the fine specimens, **Figure 4.2b**, there is little difference in the average directional strain at the final measurement, while there is a variety in the average directional strain values in the coarse specimens, **Figure 4.2a**. The values for the average directional strains can be seen in **Table 4.1** below. The variance for each direction is also

Table 4.1: Equivalent Final Average Directional Strain

	Direction X	Direction Y	Direction Z	Variance	Total Variance
Coarse Confined	0.032	0.128	0.13	$2.1x10^{-3}$	$1.9x10^{-3}$
Coarse Unconfined	0.02	0.057	0.083	$6.7x10^{-4}$	
Fine Confined	0.052	0.085	0.076	$1.9x10^{-4}$	$1.6x10^{-4}$
Fine Unconfined	0.054	0.053	0.06	$9.6x10^{-6}$	

displayed and is discussed in the following paragraph.

Notice, in **Table 4.1**, that the variance between the coarse specimen's final average directional strains are more than ten times larger than the variance between the fine specimen's final average directional strains. In addition, the coarse specimens have larger directional variances than the directional variances of the fine specimens. The similar directional strain observed in the fine specimen can be attributed to the fact noted by Smaoui et al. (2014) that aggregates with a larger surface area tend to produce more ASR

gel. The smaller nature of fine aggregates means they are more likely to have similar surface areas in all directions, see **Figure 4.3** for a depiction of the fine aggregate used to the coarse aggregate used in testing. Also, the gradation of fine aggregates (see **Chapter 3**) is much smaller than the gradation of coarse aggregates, which verifies that the consolidation of aggregates in a certain direction would not matter in the case of reactive fine aggregates. In each direction, the fine aggregates have similar surface areas, while

Non-Reactive Coarse   *Non-Reactive Fine*   *Reactive Coarse*   *Reactive Fine*

Figure 4.3: *Aggregates used in Testing*

coarse aggregates are more likely to have different surface areas when oriented in different ways due to their larger gradation and sizes. This may explain the large variation in average directional strain in **Figure 4.2a** as opposed to the smaller variation in the fine specimen, shown in **Figure 4.2b**. This phenomenon is also the reason that the largest directional variance is observed in the confined coarse specimen. The anisotropic gel expansion of confined concrete leads to large expansions in certain directions (Y and Z in this case) and small expansions in others (X in this case). The unconfined coarse specimen still experiences the anisotropic expansion, but the lack of a boundary condition leads to a smaller variance than the confined specimen. The unconfined fine specimen shows the

smallest variance between directions; therefore, the unconfined fine specimen exhibits isotropic expansion.

4.3: Acoustic Emission

It is important to reiterate that the data presented in this chapter is representative of ASR specimens under an accelerated expansion process as they were placed in a chamber to expedite the reaction's process speed. Dunant et al. (2012) outlined that aggregate size affects ASR in the preliminary life of concrete as opposed to the later stages of deterioration. Thus, data being discussed is only from the first 210 days of testing, for each coarse specimen, and 233 days of testing, for each fine specimen. The results are representative of early stage ASR damage. Above, in **Figure 4.4** the cumulative signal strengths of each specimen along with amplitude hits are plotted over the duration of 300 days for the coarse specimens and 233 days for the fine specimens.
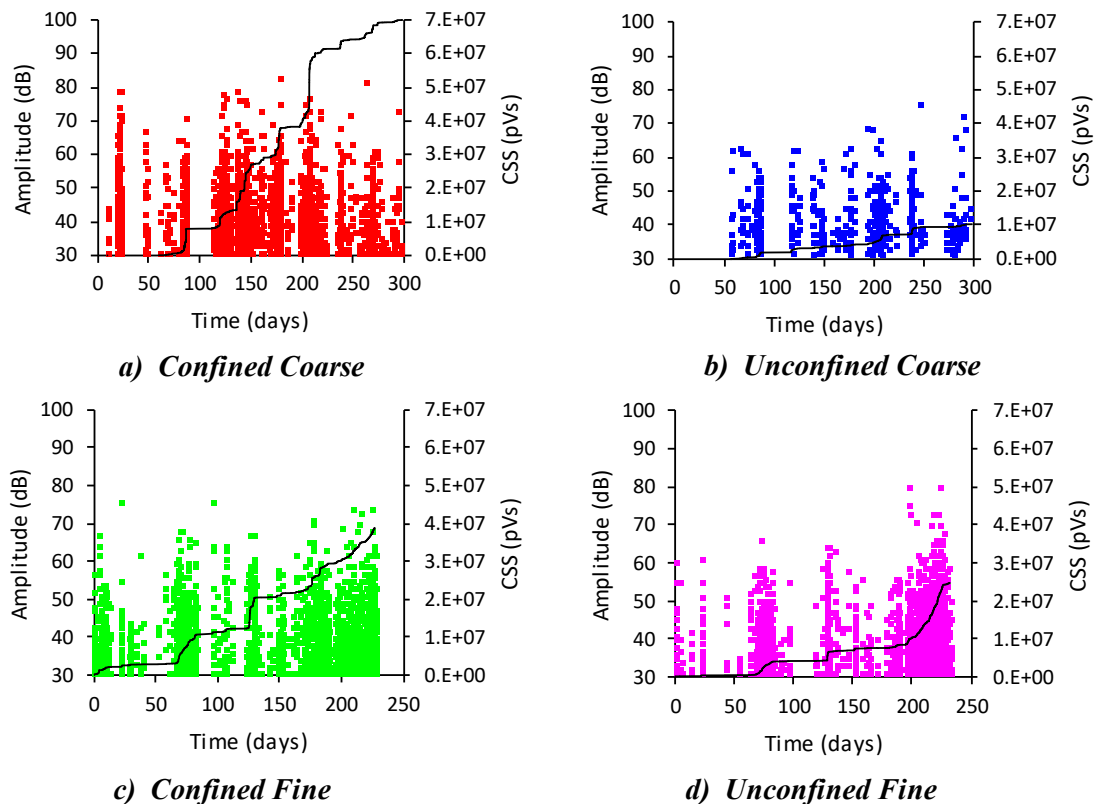

a) Confined Coarse

b) Unconfined Coarse

c) Confined Fine

d) Unconfined Fine

Figure 4.4: *CSS and Amplitude versus Time*

44

4.3.1: Fine Specimens

As seen in **Figure 4.4** the two reactive fine aggregate specimens gathered a significant amount of acoustic emission data over the course of the test. The confined specimen accrued slightly more damage indication than the unconfined specimen. However, the difference between the final cumulative signal strength (CSS) of the two specimens is only 58%. The similar amount of data between the two specimens correlates with confinement playing a small role in the damage mechanisms of reactive fine aggregate.

4.3.2: Acoustic Emission Comparison

In order to accurately compare the acoustic emission data between tests, it is important to compare the data in terms of active days. This must be done because 1 day of testing the coarse specimens is not necessarily equal to one day of testing the fine specimens. Over the course of several months each test had its own run of problems, which is why showing the data in terms of days can be misleading. Although, the above plots in **Figure 4.4** do accurately show the magnitude of damage that was accrued in the chamber over a given number of days, **Figure 4.5** below is more accurate for comparison between the two tests. Like the strain section, 233 days of fine testing is equivalent to 210 days of coarse testing. The two coarse specimens are plotted until 210 days because a strain measurement was made on that day, so the strain is more accurate than it would be on a day between measurements. **Figure 4.5** represents the acoustic emission data for all the
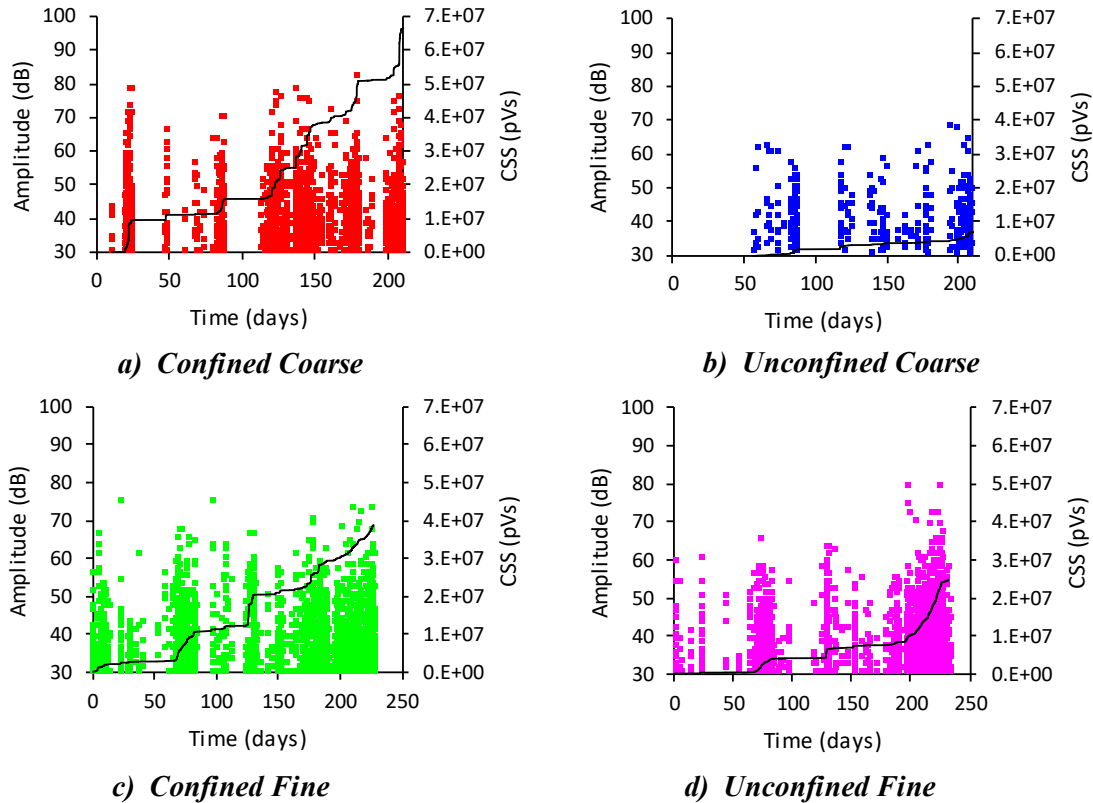
45

a) Confined Coarse *b) Unconfined Coarse*

c) Confined Fine *d) Unconfined Fine*

Figure 4.5: *CSS and Amplitude versus Adjusted Time*

specimens at the most accurate comparison point. It is also important to note that the data is not plotted versus active days, so the gaps observed in **Figure 4.5** may represent long periods of chamber maintenance or no testing, or little damage.

The values of the cumulative signal strength at the final day plotted are of interest in this thesis. In both cases the confined specimens accumulate more data, or more activity, than the unconfined specimen. This phenomenon is explained by Soltanghareai et al. (2020). However, when analyzing this relationship with different reactive aggregate sizes, a new trend is apparent. The phenomenon shown above, using acoustic emission, has not been described in previous literature. In early stages of ASR expansion, the two specimens with reactive fine aggregates have relatively similar cumulative signal strengths (CSS), while the two reactive coarse aggregate specimens have a relatively large difference in

CSS. The reactive fine aggregate concrete experiences a small 58% difference in CSS (a difference of nearly 14 million pVs) between the two unconfined and confined specimens, while the reactive coarse aggregate concrete experiences a 543% difference in CSS (a difference of nearly 50 million pVs) between the two specimens. With a much smaller difference in CSS, the fine aggregate concrete proves to be significantly less affected by boundary conditions, in particular reinforced steel, than the coarse aggregate concrete. The expansion of gel surrounding fine aggregates is less affected by boundary conditions and **Figure 4.5** shows this. In the unconfined fine specimen, there may be more AE activity because ASR gel that surrounds fine aggregates can expand similarly in all directions, no matter the boundary condition. The increase in AE activity can represent the presence of more microcracks and acoustic activity inside the unconfined fine specimen than the unconfined coarse specimen, even though the expansions are identical.

Expansion has typically been the most researched result of ASR degradation. However, the results in **Figure 4.4** show that expansion does not necessarily fully represent early ASR damage. At 233 days in the RFAC and at 210 days in the RCAC both the unconfined specimens show a .16% volumetric expansion (**Figure 4.1**). At 233 days the unconfined fine specimen exhibits a CSS nearly of 3.1 times greater than that of the unconfined coarse specimen. The significant difference between the unconfined specimens is important because previous literature has described a large difference in ASR expansion based on aggregate size; Multon et al. (2010) describes a difference up to seven times. similar volumetric strains the confined coarse specimen does in fact show a greater cumulative signal strength than the confined fine specimen, but the opposite is true for the

unconfined specimens. See **Chapter 4.6** for a more in-depth comparison of evaluation methods.

4.4: Crack Growth

As described in the experimental setup in **Chapter 3**, surface cracks were monitored and measured each time the specimens were taken out of the chamber for strain measurements. The first appearance of a surface crack, for the fine specimen testing, came on the September 25th (165 days after the specimens were placed in the chamber) measurement. The unconfined specimen had cracking, but on that day the confined fine specimen did not show any visual surface cracks. The coarse specimen crack measurements were completed in a similar manner. After 146 days the specimens began showing surface cracking and measurements were taken on subsequent strain measurement days.
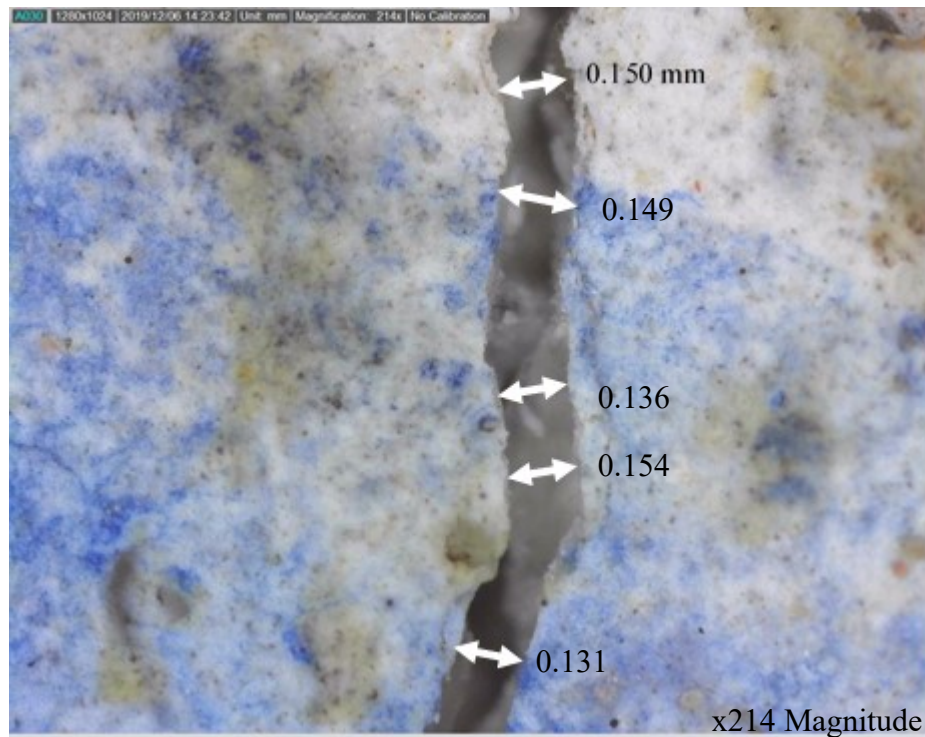

Figure 4.6: *Confined Fine Crack 3 Width*

The cracks were measured using the DinoScope software. In order to reduce error, each crack measurement is an average of at least three different widths of the same crack. **Figure 4.6** exemplifies the software used to determine crack widths for each crack.

Each measurement was documented and is averaged to determine the width of each crack on the specimens. Each specimen's cracks were kept track of, and the measurements can be seen in the plots below. **Figure 4.7a** and **Figure 4.7b** below show the maximum and average crack width on the coarse specimens up to 210 days in the chamber, while **Figure 4.7c and Figure 4.7d** show the maximum and average crack width on each specimen over the duration of the test (233 days). Still, as mentioned, 210 days of
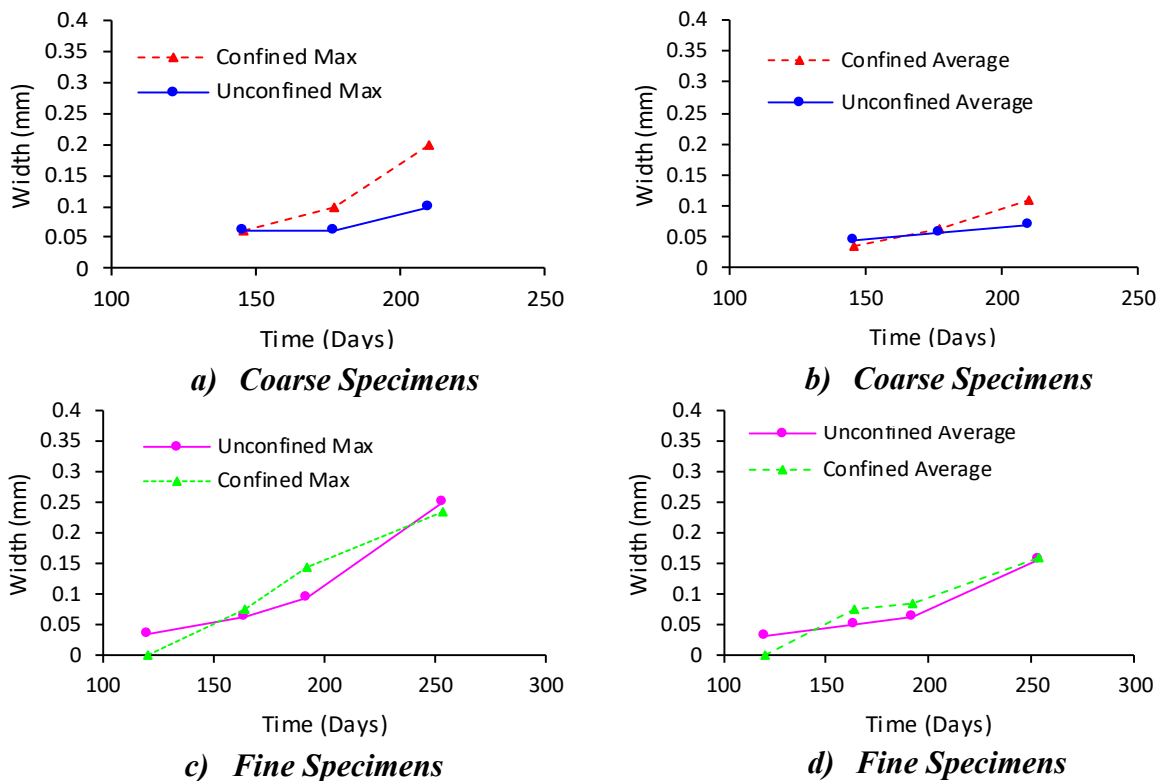

a) Coarse Specimens

b) Coarse Specimens

c) Fine Specimens

d) Fine Specimens

Figure 4.7: *Maximum and Average Crack Widths*

a) *Unconfined Fine at 233 Days*

b) *Confined Fine at 233 Days*

c) *Confined Coarse at 269 Days*

d) *Unconfined Coarse at 269 Days*
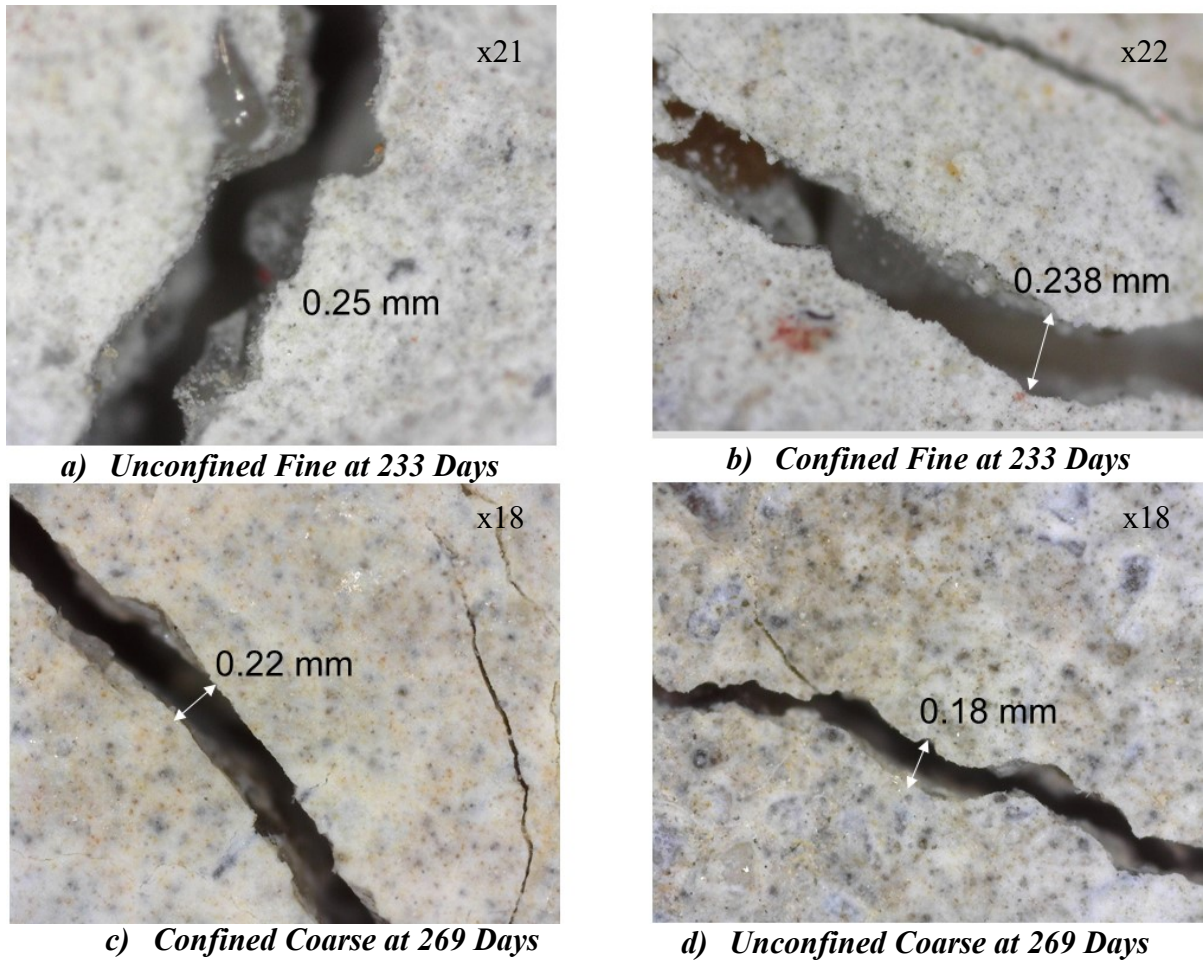
Figure 4.8: Examples of Cracks on Concrete Surfaces

coarse testing is like 233 days of fine testing, **Table 4.2** displays the maximum crack widths

of each specimen, and **Figure 4.8** shows examples of the cracks on the surface

of the specimens. Additionally, all the measurements for the coarse specimens were only

taken from the top surface of the specimen.

Table 4.2: Maximum and Average Crack Widths

	Confined Coarse	Unconfined Coarse	Confined Fine	Unconfined Fine
Average Final Crack Width (mm)	0.108	0.069	0.159	0.158
Maximum Crack Width (mm)	0.2	0.1	0.235	0.25

www.manaraa.com

It is important to note that the maximum crack widths are not necessarily from the a single crack. For example, if the first identified crack has the largest width of all cracks on the specimen for one measurement, but on the next measurement day crack one does not have the largest width, then whatever crack width is the largest on the specimen is used as the maximum for that day. The magnification for each picture is also not necessarily similar; however, the measurements are accurate as the measurements take into account the different magnifications.

4.4.1: Fine Specimen

The fine specimens have very similar crack sizes throughout the duration of testing, and the unconfined specimen has the largest crack width of all the specimens. These results align with previous sections and further enforce that boundary conditions play a small roll for reactive fine aggregates. This is evident in the small difference between the maximum widths and average widths of the fine aggregate specimens.

4.4.2: Crack Growth Comparison

Notice in **Table 4.2** that the reactive fine aggregate specimens show larger averages and maximum crack widths than the reactive coarse aggregate specimen. These results are consistent with the acoustic emission and strain data presented in the previous section, except the maximum crack width seen was not in the confined coarse aggregate specimen. However, the maximum crack width of the coarse specimen is close to the maximums in the fine concrete. Opposite to the coarse testing, the fine testing resulted in a larger number of cracks in the unconfined specimen as compared to the confined specimen. The difference between the maximum crack widths confined and fine specimens is also of interest because it further highlights the correlation between boundary condition and aggregate size. Analyzing **Figure 4.7** it is evident there is a smaller difference between the

maximum and average crack widths in the fine specimens than there is in the coarse specimens. This phenomenon coincides with the data shown in the acoustic emission section, where the unconfined fine specimen showed damage more similar to its confined counterpart than the unconfined coarse specimen showed as compared to its confined counterpart. The unconfined reactive fine aggregate concrete's maximum cracks are of similar widths when compared to the confined reactive fine aggregate concrete's (6% difference); however, the opposite is true when analyzing the coarse specimen's maximum crack widths (100% difference). Additionally, this trend is also apparent in the average crack widths of the entire surface of the concrete. The difference between the two fine specimens is significantly smaller than the difference between the two coarse specimens (.6% different to 38% different, respectively).

4.5: Ultrasonic Pulse Velocity

Ultrasonic pulse velocity (UPV) is another metric that can be used to understand the damage mechanisms inside concrete. The speed at which the pulse travels through the concrete is of interest. Based off initial control measurements, if a wave travels the same distance (the width of the concrete), at a slower speed, than the inside of the concrete is more degraded; therefore, it has more microcracks and damage, than it originally did. The direction of measurement of the wave travels is also of importance because it will outline how certain boundary conditions affect the wave speed. **Table 4.3** shows the average time taken to travel through the concrete in each direction, and **Figure 4.9** is a graphical depiction of the wave speeds of each fine specimen in different directions.

As seen in the acoustic emission data, strain data, and crack growth data, it remains evident from **Figure 4.9** that there is a similar amount of degradation when comparing the unconfined specimen to the confined specimen using UPV data. It is also clear that the

52

Table 4.3: *Average Speed and Direction of Pulse Wave*

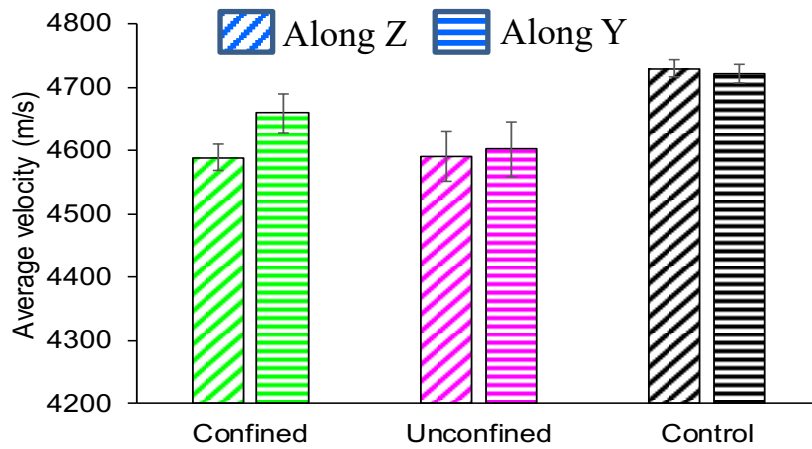|	Average Time (microseconds)	Average Speed (m/s)
Confined along Width	65.4 ± 0.58	4659 ± 21
Confined along Height	67.8 ± 0.70	4588 ± 31
Unconfined along Width	66.9 ± 0.65	4602 ± 39
Unconfined along Height	67.1 ± 0.75	4591 ± 43
Control along Width	64.6 ± 0.44	4722 ± 14
Control along Height	64.4 ± 0.44	4729 ± 14

Figure 4.9: *Average Speed of Pulse Wave by Direction in Fine Specimen*

wave speeds experienced by the control specimen are much higher than the wave speed of the reactive specimens. Therefore, UPV can accurately detect microcracking and interior damage due to ASR. The unconfined fine specimen has a slighly lower wave speed in the width (Y direction, by 1.23%) and a slightly larger wave speed in the height (Z direction, .05% difference), than the confined specimen. Therefore, in the Y direction there may be more microcracks and degradation in the unconfined specimen, but in the Z direction the opposite is true. The isotropic expansion of the fine aggregate ASR gel is what allows for this phenomenon to take place. There is little effect from the confinement, so in both specimens there is a similar wave speed and similar amount of damage. Therefore, it is

accurate to see small differences in wave velocity when comparing the damage in each direction of each specimen.

The direction of the UPV test is also important because the results still show how the confinement affects ASR internal expansion. The unconfined specimen shows very similar wave velocities in both observed directions, while the confined specimen shows a larger difference. This larger difference displays the effect that takes place due to the presence of a bounday condition.

Since the UPV results are very similar when comparing the unconfined and confined specimen, the hypothesis of this thesis is further solidified. Even with the error that can come with UPV testing, there is a clear trend exhibiting the emphasis confinement puts on expansion and degradation. In addition, the isotropic expansion of the ASR gel in reactive fine aggregate concrete is apparent, since the wave speeds between specimens are within 1.5% of each other.

4.6: Evaluation Methods Comparison

The methods investigated in this thesis each have their own pros and cons, but an evaluation of their effectiveness can help to further the body of knowledge surrounding ASR in concrete. Each of the testing methods is different, so in order to compare them, one must look at similar parameters in each. Each method has a relationship to the control specimens and each method has an amount of time before data is accrued. In terms of this thesis, a large percent difference between the final control data and the reactive specimen final data would mean that method is more effective, while a larger duration to acquire initial data points would mean that method is less effective. Therefore, dividing the percent difference by the time it takes to acquire meaningful data would yield an effectiveness value. This effectiveness value can then be normalized by taking each method and each

54

specimen (16 total values) and dividing each individual effectiveness by the maximum effectiveness. Averaging these values by test method will yield an average normalized effectiveness for each method (out of 100%), and show which evaluation method is the most effective.

4.6.1: Strain

The control specimens' volumetric strain is plotted in **Figure 4.10**. As previously mentioned, the specimen that was tested alongside the reactive coarse specimens (the unconfined control) experienced some shrinkage, while the confined specimen little experienced initial expansion. The final volumetric strains for the reactive
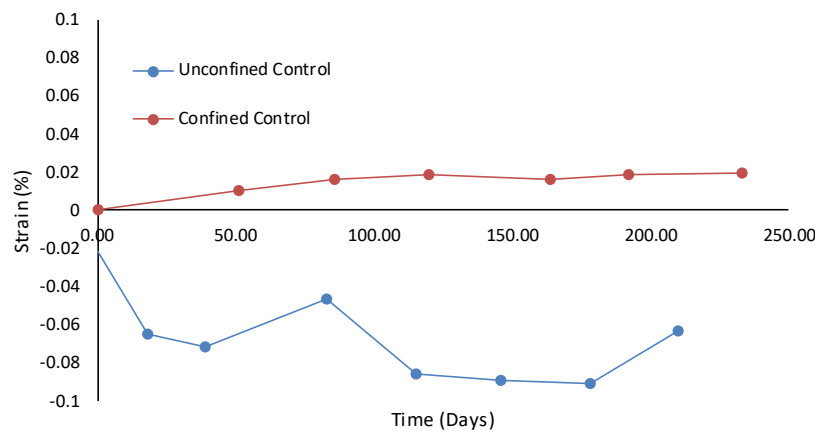
Figure 4.10: Control Specimen's Volumetric Strain

specimens are clearly much different than the control specimens, which is expected in ASR specimens. However, as stated at the beginning of this chapter, another area of interest is the amount of difference that is shown by volumetric strain data. **Table 4.4** shows the percent difference in volumetric strains from the control for each reactive specimen. It is apparent from **Table 4.4** that strain measurements clearly represent the effects of early ASR expansion because there are relatively large differences in strain when comparing the reactive specimens to the control specimens. The control specimens reflect concrete that does not experience ASR; therefore, large percent differences reflect how effective each

55

evaluation method is. In this case, strain measurements are the evaluation method and the results enforce strain as a strong evaluation method for early ASR.

Table 4.4: Percent Differences (Strains) from Control to Reactive Specimens

	Confined Coarse	Confined Fine	Unconfined Coarse	Unconfined Fine
Difference from Control (%)	1403	1006	267	267

4.6.2: Acoustic Emission

The control specimens' AE data is shown in **Figure 4.11**. The confined control specimen was tested with unreactive aggregates and placed in the chamber while the reactive fine aggregate specimens were tested, so it is plotted for 233 days. The unconfined
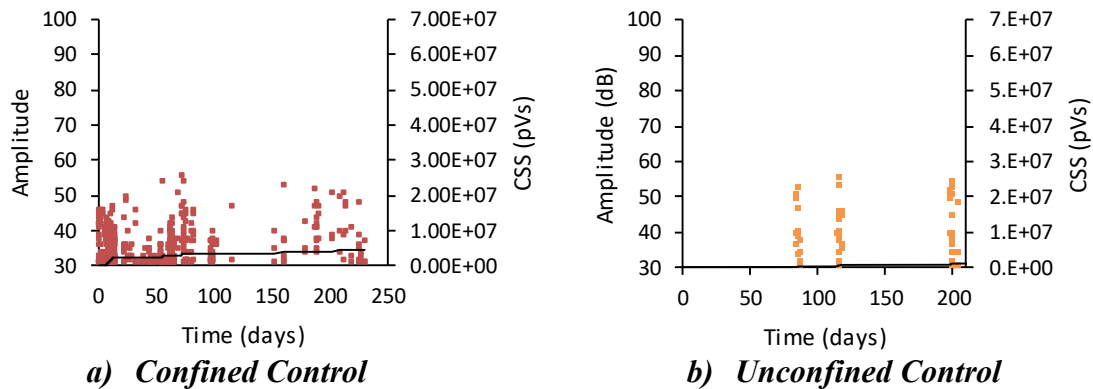

a) *Confined Control*   b) *Unconfined Control*

Figure 4.11: Cumulative Signal Strength and Amplitude vs Adjusted Time (Controls)

control specimen was tested with unreactive aggregates as well but tested while the reactive coarse aggregates were in the chamber. The unconfined control specimen is plotted for 210 days. The final CSS for the confined control specimen was 4.6×10^6 pVs, and the final CSS for the unconfined control specimen was 1.8×10^6 pVs. In comparison to the reactive fine and coarse aggregate specimens, acoustic emission proves to be very effective at detecting early stages of ASR. The percent increases can be seen in **Table 4.5**. The smallest change

56

is 494%. Therefore, acoustic emission, and more particularly cumulative signal strength, is a strong identifier of early ASR damage.

Table 4.5: Percent Differences (CSS) from Control to Reactive Specimens

	Confined Coarse	Confined Fine	Unconfined Coarse	Unconfined Fine
Difference from Control (%)	1360	742	494	1290

4.6.3: Crack Growth

Crack growth measurements are very representative of how damaged concrete is in early stages of ASR, as well as other damage mechanisms. However, in this thesis there were no visual cracks seen on the control specimens, so in order to compare the effectiveness of crack growth measurements to the other evaluation methods one must observe the timeframe in which cracks began to appear on the reactive specimens. In the previous sections the effectiveness of each method was dependent on the percent difference in reactive data vs control data. Since there are no cracks on the control specimen, there needs to be another comparison metric. This metric is the time in which it took for cracks to be visualized. **Table 4.6** shows how long it took for meaningful data to be seen in each reactive specimen. Investigating the amount of time before data can be gathered is an important factor when assessing effectiveness for different evaluation methods. The discussion about the methods comparisons can be seen at the end of this section.

Table 4.6: Amount of Days Prior to First Meaningful Data

	Confined Coarse	Confined Fine	Unconfined Coarse	Unconfined Fine
Days to First Crack	146	164	146	120
First CSS Event (Days)	82	63	86	69
First Strain Change (Days)	115	51	83	51

4.6.4: UPV

Figure 4.9 shows the relationship between the wave speeds of each reactive fine aggregate as well as the confined control wave speed. The wave speed of the coarse specimens will not be discussed in this section because there were no intermediate wave speed tests done for the coarse specimens, and the timeline would not be accurate for comparison. Therefore, the best investigation method for the UPV test is the percent difference in wave speed by direction between the confined fine specimen and the confined control. **Table 4.7** shows this percent difference. See the following subsection for a comparison of all the evaluation methods.

Table 4.7: Percent Difference (Wave Speed) from Control to Fine

	Confined Fine (Z)	Confined Fine (Y)
Percent Difference in Wave Speed (%)	3	1.33

Chapter 4.6.5: Effectiveness Comparison

Generally, all the aforementioned evaluation methods detect early ASR degradation to some extent, and they can all be utilized in the field. However, the effectiveness of each method differs, and the investigative research above outlines this. The contrast begins with understanding the difference in degradation metrics (acoustic emission hits, expansion, etc.) from beginning to end. The non-destructive test methods do not have data that represents any beginning because all initial data would be zero (no time for ASR would yield zero AE hits, zero expansion, and no crack formations). So, to counter this problem, the reactive data is compared to the data received from the non-reactive control specimens, which can represent structures not affected by ASR. Also, the methods being contrasted do not use similar units, so the best way to compare them is via percentages. The percent differences between these specimens helps to yield an understanding of the effectiveness

of each test method in comparison to each other. Effectiveness is first calculated by percent differences divided by time, and then it is normalized to percentages for comparison.

Effectiveness, in order to accurately compare the four different methods, is defined as each methods ability to monitor ASR in concrete in terms of severity and time. Severity is represented by the percent difference in final data between control specimens and reactive specimens. Time is represented by the amount of time each method needed in order to show meaningful data. Taking these considerations into account the author has developed a rank based on the results show and it is as follows: acoustic emission reflects early ASR most effectively (of the 4 methods considered), expansion/strain measurements are the second most effective, crack measurements are third, while UPV is the least effective, see **Figure 4.12** for the normalized average effectiveness comparison. Acoustic emission has the largest minimum percent difference when comparing the acoustic events are happening very early and very often. Strain measurements are also very effective when it comes to early ASR detection; however, from the results discussed above it is clear that
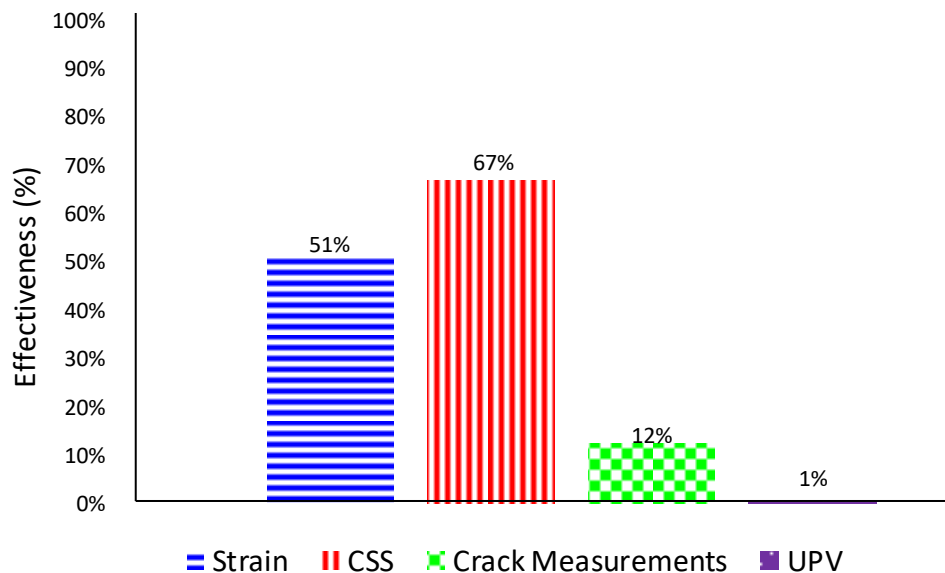

Figure 4.12: *Normalized Average Effectiveness of Each Method*

expansion may not tell the whole story. For example, when each reactive unconfined specimen had the same volumetric strain (at .16%) the CSS's were nearly 3.2 times different. So, acoustic emission may have the ability to understand interior degradation better than strain measurements. Crack measurements are incredibly effective, but they are third in this ranking system because of how long they may take to appear. While microcracks are forming inside the concrete it is very possible ASR goes unnoticed if a sole evaluation method is to wait for cracks to appear. Lastly, UPV is ranked last in this system because of its very low difference between the control wave speed and reactive specimen wave speed. UPV uses a low frequency pulse which may attribute to this low difference. UPV is not as reliable as the other methods discussed (Sargolzahi 2009).

CHAPTER 5

Summary and Conclusions

5.1: Summary of Test

An accelerated alkali-silica reaction (ASR) test was conducted on several concrete specimens with different stress boundary conditions and different reactive aggregates in order to understand the damage mechanisms that occur in the early stages of ASR. Multiple non-destructive testing was investigated. Simply, ASR is a chemical reaction that begins when concrete is initially mixed. It creates a microscopic gel that forms on the surface of interior aggregates inside concrete. This gel is hydroscopic and will expand as it is exposed to moisture, so ASR occurs often in areas with high humidity. Typically, ASR affected structures includes dams, ocean side structures, and nuclear power plants. The expansion from the gel forms internal microcracks and variable stress as it creates pressure as it expands.

The effect of aggregate size on ASR damage mechanisms has been discussed in literature and this is present from authors like Multon et al., and Dunant et al. However, analyzing the relationship using non-destructive methods using non-destructive methods such as acoustic emission is not present in the literature. Additionally, the addition of different confinement conditions provides an area of untapped potential for the growth of knowledge of ASR and concrete.

Acoustic emission (AE) is a recent and effective non-destructive method being used to understand damage in many areas of research. It is effective for concrete tests because it is highly sensitive and can detect small releases of energy. AE incorporates placing piezoelectric sensors on surfaces of specimens to determine the energies, frequencies, locations, and more of a variety of events that happen inside a structure. Acoustic emission is useful in concrete applications because it has the potential to detect microcracks and the growth of damage on the interior of concrete, non-destructively; therefore, AE can be

www.manaraa.com

incredibly useful in understanding the damage mechanisms of ASR. In addition, strain measurements, crack growth measurements, and UPV analysis were also investigated as evaluation methods to analyze ASR damage mechanisms.

The experimental setup for this thesis consisted of 6 concrete test specimens, each with differing stress boundary conditions and reactive aggregate. There were 2 reactive coarse aggregate specimens, 2 reactive fine aggregate specimens, and 2 controls for each group. Each of the reactive aggregate groups had an unconfined and confined specimen. A confined specimen is a concrete specimen with reinforcing steel imposed inside, and unconfined has no reinforcement. The specimens were cast as rectangular beams with dimensions of 12" x 12" x 44". Each specimen was placed in a high temperature and high relative humidity chamber for eight, or more, months to accelerate the ASR reaction. The specimens were constantly monitored by AE sensors while in the chamber. Monthly length change (strain) measurements were completed to gather expansion information, and once cracks began to form on the surfaces, the crack widths were measured and noted. In addition, an ultrasonic pulse velocity (UPV) test was completed at the beginning and end of the reactive fine aggregate specimen testing as another method to determine the interior degradation change experienced. The group of reactive fine specimens were tested subsequently after the reactive coarse specimens had resided in the acceleration chamber for nearly two years.

5.2: Strain

In terms of strain and expansion, the average directional expansions of the reactive coarse aggregate specimens varied greatly, depending on directions. The reactive fine aggregate specimens had a very small variance when comparing directions. In conclusion, the strains of each specimen show that reactive fine aggregate concrete's

expansion is dependent on confinement; it will expand in an isotropic manner without reinforcement, but in an anisotropic manner with reinforcement. Alternatively, the reactive coarse aggregate concrete expands in an anisotropic manner, no matter the confinement structure.

5.3: Acoustic Emission

In the acoustic emission results, the addition of a boundary condition leads to a large difference in ASR related damage between the two coarse specimens, but leads to a relatively small difference in ASR damage between the two fine specimens. The acoustic emission data shown is additional metric that describes a conclusion to this thesis' objective of understanding the relationship between aggregate size and reinforcement: reactive coarse aggregate concrete expansion is affected by confinement more than reactive fine aggregate expansion is affected. This phenomenon could be a result of the isotropic expansion seen in the unconfined fine specimen.

5.4: Crack Growth

The crack meassurement results show that it is evident that reactive fine aggregate's ASR products are significantly less affected by boundary conditions than reactive coarse aggregate's ASR products are. Reactive coarse aggregate concrete exhibits greater large widths when a boundary condition is imposed, but small crack widths with the absence of a boundary condition. Reactive fine aggregate concrete shows similar crack widths in both cases. Clearly, the different types of expansion experienced by each type of aggregate are of importance when discussing crack growth related to ASR.

5.5: UPV

Lastly, the UPV test performed on the reactive fine aggregate concretes shows that the unconfined fine specimen exhibits isotropic expansion. The control specimen showed a much higher wave velocity through each concrete direction, which also provides information that ASR damage can be detected by UPV tests. The wave speeds of the two directions of the unconfined specimen were nearly identical, which helps to solidify the statement that unconfined reactive aggregate specimen expands in an isotropic manner.

5.6: Effectiveness of Evaluation Methods

The methods investigated in this thesis were also compared in terms of effectiveness in order to compare each evaluation method. Effectiveness in this context takes into consideration the amount of time before data is received as well as the difference in final values from the final control specimen to the reactive specimens. The rank is as follows: acoustic emission (cumulative signal strength), expansion measurements, visual crack measurements, and UPV. Acoustic emission and CSS reflect early ASR most effectively, while UPV was the least effective method of the four investigated.

5.7: Additional Conclusions

This study was completed to begin in understanding the complicated relationship between reactive aggregate size and boundary condition when exposed to ASR damage mechanisms. Additionally, it was completed to investigate the effectiveness of certain non-destructive evaluation methods. A clear relationship is shown in the results of this thesis, but there is more that can be understood through further research on this subject. Acoustic emission has endless possibilities and should be further used in ASR research. Additionally, the subject of interest in this thesis should also be investigated using other methods of testing like coring and petrography.

REFERENCES

Abdelrahman, M., Elbatanouny, M. K., Ziehl, P., Fasl, J., Larosche, C. J., & Fraczek, J. (2015). Classification of alkali–silica reaction damage using acoustic emission: A proof-of-concept study. *Construction and Building Materials, 95*, 406-413. doi:10.1016/j.conbuildmat.2015.07.093

Anay, R., Cortez, T. M., Jáuregui, D. V., Elbatanouny, M. K., & Ziehl, P. (2016). On-site acoustic-emission monitoring for assessment of a prestressed concrete double-tee-beam bridge without plans. *Journal of Performance of Constructed Facilities, 30*(4), 04015062. doi:10.1061/(asce)cf.1943-5509.0000810

ASTM C150 / C150M-19a, Standard Specification for Portland Cement, ASTM International, West Conshohocken, PA, 2019, www.astm.org

ASTM C227-10, Standard Test Method for Potential Alkali Reactivity of Cement-Aggregate Combinations (Mortar-Bar Method) (Withdrawn 2018), ASTM International, West Conshohocken, PA, 2010, www.astm.org

ASTM C289-07, Standard Test Method for Potential Alkali-Silica Reactivity of Aggregates (Chemical Method) (Withdrawn 2016), ASTM International, West Conshohocken, PA, 2007, www.astm.org

ASTM C295 / C295M-19, Standard Guide for Petrographic Examination of Aggregates for Concrete, ASTM International, West Conshohocken, PA, 2019, www.astm.org

ASTM E750-15, Standard Practice for Characterizing Acoustic Emission Instrumentation, ASTM International, West Conshohocken, PA, 2015, www.astm.org

ASTM E1316-20, Standard Terminology for Nondestructive Examinations, ASTM International, West Conshohocken, PA, 2020, www.astm.org

Benedetti, M. D., Loreto, G., Matta, F., & Nanni, A. (2014). Acoustic emission historic index and frequency spectrum of reinforced concrete under accelerated corrosion. *Journal of Materials in Civil Engineering, 26*(9), 04014059. doi:10.1061/(asce)mt.1943-5533.0000954

Dunant, C. F., & Scrivener, K. L. (2012). Effects of aggregate size on alkali–silica-reaction induced expansion. *Cement and Concrete Research, 42*(6), 745-751. doi:10.1016/j.cemconres.2012.02.012

Elbatanouny, M. K., Anay, R., Abdelrahman, M. A., & Ziehl, P. (2019). Acoustic emission measurements for load testing. *Load Testing of Bridges,* 169-198. doi:10.1201/9780429265969-6

Elbatanouny, M. K., Ziehl, P. H., Larosche, A., Mangual, J., Matta, F., & Nanni, A. (2014). Acoustic emission monitoring for assessment of prestressed concrete beams. *Construction and Building Materials, 58,* 46-53. doi:10.1016/j.conbuildmat.2014.01.100

Farnam, Geiker, M. R., Bentz, D., & Weiss, J. (2015). Acoustic emission waveform characterization of crack origin and mode in fractured and ASR damaged concrete. *Cement and Concrete Composites, 60,* 135-145. doi:10.1016/j.cemconcomp.2015.04.008

Hillerborg, A., Modéer, M., & Petersson, P. (1976). Analysis of crack formation and crack growth in concrete by means of fracture mechanics and finite elements. *Cement and Concrete Research, 6*(6), 773-781. doi:10.1016/0008-8846(76)90007-7

Hobbs, B., & Kebir, M. T. (2007). Non-destructive testing techniques for the forensic engineering investigation of reinforced concrete buildings. *Forensic Science International, 167*(2-3), 167-172. doi:10.1016/j.forsciint.2006.06.065

Jones, M. K. (2013). Structural health monitoring of concrete systems (Order No. 1550852). Available from Dissertations & Theses @ University of South Carolina; ProQuest Dissertations & Theses Global. (1496772411).

Jóźwiak-Niedźwiedzka, D., Dąbrowski, M., Gibas, K., Antolik, A., & Glinicki, M. A. (2018). Alkali-silica reaction and microstructure of concrete subjected to combined chemical and physical exposure conditions. *MATEC Web of Conferences, 163*, 05009. doi:10.1051/matecconf/201816305009

Kawamura, M., & Fuwa, H. (2003). Effects of lithium salts ON ASR gel composition and expansion of mortars. *Cement and Concrete Research, 33*(6), 913-919. doi:10.1016/s0008-8846(02)01092-x

Kumar S., Arumugam, V., Sengottuvelusamy, R., Srinivasan, S., & Dhakal, H. (2017). Failure strength prediction of glass/epoxy composite laminates from acoustic emission parameters using artificial neural network. *Applied Acoustics, 115*, 32-41. doi:10.1016/j.apacoust.2016.08.013

Liaudat, Carol, I., López, C. M., & Saouma, V. E. (2018). ASR expansions in concrete under triaxial confinement. *Cement and Concrete Composites, 86*, 160-170. doi:10.1016/j.cemconcomp.2017.10.010

Lokajíček, T., Přikryl, R., Šachlová, Š, & Kuchařová, A. (2017). Acoustic emission monitoring of crack formation during alkali silica reactivity accelerated mortar bar test. *Engineering Geology, 220*, 175-182. doi:10.1016/j.enggeo.2017.02.009

Thomas, M., Folliard, K., Fournier, B., Rivard, P., Drimalas, T., & Garber, S. (2013). *Methods for Evaluating and Treating ASR-Affected Structures: Results of Field Application and Demonstration Projects – Volume II: Details of Field Applications and Analysis* (Rep. No. FHWA-HIF-14-0003). Federal Highway Administration.

Malone, C., Hu, J., Giannini, E., & Zhu, J. (2019) ASR Specimen Design and Fabrication. *Prepared for NEUP Project 16-10214: Online Monitoring System for Concrete Structures Affected by Alkali-Silica Reaction (ASR).*

Mo, X. (2005). Laboratory study OF LiOH in INHIBITING ALKALI–SILICA reaction at 20 °C: A contribution. *Cement and Concrete Research, 35*(3), 499-504. doi:10.1016/j.cemconres.2004.06.003

Morenon, P., Multon, S., Sellier, A., Grimal, E., Hamon, F., & Bourdarot, E. (2017). Impact of stresses and restraints on asr expansion. *Construction and Building Materials, 140*, 58-74. doi:10.1016/j.conbuildmat.2017.02.067

Multon, Cyr, M., Sellier, A., Diederich, P., & Petit, L. (2010). Effects of aggregate size and Alkali content ON Asr expansion. *Cement and Concrete Research, 40*(4), 508-516. doi:10.1016/j.cemconres.2009.08.002

Multon, Cyr, M., Sellier, A., Leklou, N., & Petit, L. (2008). Coupled effects of aggregate size and Alkali content ON Asr expansion. *Cement and Concrete Research, 38*(3), 350-359. doi:10.1016/j.cemconres.2007.09.013

Rajabipour, F., Giannini, E., Dunant, C., Ideker, J. H., & Thomas, M. D. (2015). Alkali–silica reaction: Current understanding of the reaction mechanisms and the knowledge gaps. *Cement and Concrete Research, 76*, 130-146. doi:10.1016/j.cemconres.2015.05.024

Rep. No. FHWA-HIF-14-0003 (2013).

Saouma, V. E., & Hariri-Ardebili, M. A. (2014). A proposed aging management program for alkali silica reactions in a nuclear power plant. *Nuclear Engineering and Design, 277*, 248-264. doi:10.1016/j.nucengdes.2014.06.012

Sargolhazi, M., Rivard, P., & Rhazi, J. (2009, June 30). Evaluation of residual reactivity of concrete cores from ASR-affected structures by non-destructive tests. *Non-Destructive Testing in Civil Engineering.*

Shahidan, S., Pulin, R., Bunnori, N. M., & Holford, K. M. (2013). Damage classification in reinforced concrete beam by acoustic emission signal analysis. *Construction and Building Materials, 45*, 78-86. doi:10.1016/j.conbuildmat.2013.03.095

Soltangharaei, V., Anay, R., Hayes, N., Assi, L., Pape, Y. L., Ma, Z., & Ziehl, P. (2018). Damage mechanism evaluation of large-scale concrete structures affected by alkali-silica reaction using acoustic emission. *Applied Sciences, 8*(11), 2148. doi:10.3390/app8112148

Soltangharaei, V., Anay, R., Ai L., Giannini E., Zhu J., & Ziehl, P. (Accepted on March 5, 2020). Temporal Evaluation of ASR Cracking in Concrete Specimens Using Acoustic Emission. *Journal of Materials in Civil Engineering,* doi:10.1061/(ASCE)MT.1943-5533.0003353

Teramoto, A., Watanabe, M., Murakami, R., & Ohkubo, T. (2018). Visualization of internal crack growth due to alkali–silica reaction using digital image correlation. *Construction and Building Materials, 190*, 851-860. doi:10.1016/j.conbuildmat.2018.09.168

Virmani, P., & Faraidazar, F. (2014). *Alkali-Silica Reaction Mechanisms and Detection: An Advanced Understanding* (Publication No. FHWA-HRT-14-079). Federal Highway Administration.

Yu, J., Ziehl, P., Zárate, B., & Caicedo, J. (2011). Prediction of fatigue crack growth in steel bridge components using acoustic emission. *Journal of Constructional Steel Research, 67*(8), 1254-1260. doi:10.1016/j.jcsr.2011.03.005

Zhang, J. (2018). Investigation of relation between fracture scale and acoustic emission time-frequency parameters in rocks. *Shock and Vibration, 2018*, 1-14. doi:10.1155/2018/3057628

Ziehl, P. H. (2008). Applications of acoustic emission evaluation for civil infrastructure. Nondestructive Characterization for Composite Materials, Aerospace Engineering, Civil Infrastructure, and Homeland Security 2008. doi: 10.1117/12.779069

Ziehl, & Elbatanouny, M. (2016). Acoustic emission monitoring for corrosion damage detection and classification. *Corrosion of Steel in Concrete Structures,* 193-209. doi:10.1016/b978-1-78242-381-2.00010-9